# Theoretically based optimal large-eddy simulation

Robert D. Moser,[1,2] Nicholas P. Malaya,[2] Henry Chang,[1] Paulo S. Zandonade,[3] Prakash Vedula,[4] Amitabh Bhattacharya,[5] and Andreas Haselbacher[6]
[1]*Institute for Computational Engineering and Sciences, University of Texas at Austin, Austin, Texas 78712, USA*
[2]*Department of Mechanical Engineering, University of Texas at Austin, Austin, Texas 78712, USA*
[3]*Department of Theoretical and Applied Mechanics, University of Illinois at Urbana–Champaign, Urbana, Illinois 61801, USA*
[4]*Department of Aerospace and Mechanical Engineering, University of Oklahoma, Norman, Oklahoma 73019, USA*
[5]*Department of Chemical Engineering, University of Pittsburgh, Pittsburgh, Pennsylvania 15260, USA*
[6]*Department of Mechanical and Aerospace Engineering, University of Florida, Gainesville, Florida 32611, USA*

(Received 9 December 2008; accepted 13 September 2009; published online 23 October 2009)

Large eddy simulation (LES), in which the large scales of turbulence are simulated while the effects of the small scales are modeled, is an attractive approach for predicting the behavior of turbulent flows. However, there are a number of modeling and formulation challenges that need to be addressed for LES to become a robust and reliable engineering analysis tool. Optimal LES is a LES modeling approach developed to address these challenges. It requires multipoint correlation data as input to the modeling, and to date these data have been obtained from direct numerical simulations (DNSs). If optimal LES is to be generally useful, this need for DNS statistical data must be overcome. In this paper, it is shown that the Kolmogorov inertial range theory, along with an assumption of small-scale isotropy, the application of the quasinormal approximation and a mild modeling assumption regarding the three-point third-order correlation are sufficient to determine all the correlation data required for optimal LES modeling. The models resulting from these theoretically determined correlations are found to perform well in isotropic turbulence, with better high-wavenumber behavior than the dynamic Smagorinsky model. It is expected that these theory-based optimal models will be applicable to a wide range of turbulent flows, in which the small scales can be modeled as isotropic and inertial. The optimal models developed here are expressed as generalized quadratic and linear finite-volume operators. There are significant quantitative differences between these optimal LES operators and standard finite-volume operators, and these differences can be interpreted as the model of the subgrid effects. As with most other LES models, these theory-based optimal models are expected to break down near walls and other strong inhomogeneities. © *2009 American Institute of Physics*. [doi:10.1063/1.3249754]

## I. INTRODUCTION

In the large-eddy simulation (LES) of turbulence, the large scales of motion are identified using a low-pass filter and their dynamical evolution is computed using numerical simulation. In such simulations, the effects of the unresolved small-scale motions on the (resolved) large scales must be modeled (see Refs. 1–3 for reviews). The large-scale turbulence generally plays a dominant role in the transport of momentum, energy, heat, and chemical species in a turbulent flow and, in this context, the small (unresolved) scales are important only because of their effects on the large scales. As the small scales tend to be universal over a wide range of turbulent flows,[4] widely applicable models of small-scale interactions with the large scales can be developed. Although LES offers the promise of being a reliable tool for turbulence prediction, there are several shortcomings in most current LES formulations. In particular, they generally do not treat the effects of discretization errors[5,6] or near-wall turbulence.[7]

Recent developments in *optimal* LES (OLES) modeling[8–11] have addressed some of these issues. Of particular relevance to the current discussion is the paper of Zandonade *et al.*,[11] in which the impact of discretization error is addressed. Zandonade *et al.* pointed out that in many cases, it is the discretization that determines what large-scale information is available because the filters commonly employed for LES (e.g., Gaussian or top hat) are invertible or nearly so. Similar observations were made by Carati *et al.*[12] and similar considerations underlie the variational multiscale approach to LES.[13,14] It is also noted that the commonly proposed approach of refining the numerical discretization to reduce discretization errors, while maintaining a constant filter width, is unattractive due to the expense involved, but primarily because it does not address the fundamental issue associated with invertible filters.

Instead, Zandonade *et al.*[11] defined the LES filter to be the mapping from the infinite-dimensional space of the Navier–Stokes solutions for the turbulent flow to a finite-dimensional space of LES solutions, which can then be represented computationally without further numerical approximation. A finite-volume filter, which simply leads to a coarse finite-volume representation of the turbulent velocity, is

 

used. The momentum fluxes through the boundaries of the finite volumes, which appear in the evolution equation for the volume-averaged velocities, are then the quantities that must be modeled. In Ref. 11, the OLES technique is used to develop models for these fluxes. In this way, a model that accounts for numerical discretization as well as subgrid turbulence is obtained. A finite-volume representation is used rather than a spectral representation because the former is more easily applied to flows with complex geometries.

The performance of the coarse finite-volume OLES models was found to be quite promising in Ref. 11. In isotropic turbulence, the *a posteriori* results obtained from finite-volume OLES models were more accurate than those obtained with the dynamic Smagorinsky model using either second- or fourth-order accurate discretizations of the flux terms.

The finite-volume OLES models of Zandonade *et al.*[11] required surface and volume integrals of multipoint velocity correlations up to fourth order as input. In Ref. 11, the input correlations were obtained from well-resolved direct numerical simulations (DNSs) of isotropic turbulence, to allow the models to be evaluated in the absence of further modeling errors. However, this dependence on DNS statistical data must be eliminated if the OLES models are to be useful as a predictive tool in more general flows. The research presented here was undertaken to eliminate this need for DNS data.

Assuming that the filter width (finite-volume size) is in the inertial range and that the small scales are isotropic, the data requirements can be eased using classical theories of turbulence. In this paper, we explore generalizations of finite-volume OLES models, in which the inputs are obtained using a combination of Kolmogorov inertial range theory for second- and third-order correlations, a simple modeling ansatz for third-order three-point correlations,[15] and the quasi-normal approximation for the fourth-order velocity correlations. Since inertial range theory is valid for very high Reynolds number turbulent flows, the resulting OLES models will capture the large-scale statistical behavior of turbulent flows at very high Reynolds numbers.

The remainder of this paper is organized as follows. In Sec. II, we provide a brief overview of the OLES formalism emphasizing the required statistical inputs. The evaluation of these inputs from turbulence theory is addressed in Sec. III. The application of these theoretically based OLES models and the resulting simulations are described in Sec. IV, and the characteristics of the OLES model operators are analyzed in Sec. V. Concluding remarks are provided in Sec. VI.

## II. OPTIMAL LES

The OLES model formulation is predicated on the observation that in the absence of information about the small scales, the evolution of the simulated large scales is inherently uncertain, and can be treated as stochastic.

As described elsewhere,[8–11] the OLES process begins with the selection of a mapping (a filter) that maps the infinite-dimensional space of Navier–Stokes solutions to a computationally feasible finite dimensional space. This mapping defines the large scales to be simulated as well as the discarded small-scale information. Examples of such filters are Fourier cutoff filters and point-sampled top-hat filters. Due to the discarded information, a large-scale (filtered) field defined by such a mapping has a distribution of possible time evolutions arising from all the possible small scales that could be associated with it. In deterministic LES, a single evolution must be defined that appropriately represents this distribution.

A natural choice for the deterministic LES evolution is the average over the distribution of possible evolutions. This is written as

$$\frac{\partial \mathbf{w}}{\partial t} = \left\langle \overline{\frac{\partial \mathbf{u}}{\partial t}} \middle| \overline{\mathbf{u}} = \mathbf{w} \right\rangle, \tag{1}$$

where $\mathbf{w}$ is the LES field to be evolved, $\mathbf{u}$ is the real turbulence, $\bar{\cdot}$ is the filter operator, and $\langle \cdot | \cdot \rangle$ is the conditional average. It can be shown[8,16] that this evolution minimizes the mean-square difference between the evolutions of the LES and the filtered turbulence, and that it results in a LES that reproduces the single-time statistics of the filtered turbulence. These are precisely the properties we desire of a LES, and so Eq. (1) is called the ideal LES.

Unfortunately, the ideal LES is impractical to determine since the number of conditions defining the conditional average in Eq. (1) is the number of degrees of freedom in the LES representation (many thousands to millions). Instead, the ideal LES is formally approximated using stochastic estimation[17] to yield an "OLES" model. Models of this sort were first proposed by Adrian,[18,19] and were recently developed and tested.[8–11,20] However, these optimal models still require substantial statistical data as input. In particular, they are formulated using up to fourth-order multipoint velocity correlations, which were determined from DNSs in the cited studies. It was found that OLES models yielded very accurate LES.

For OLES to be useful, however, it is necessary that models be formulated without substantial need for DNS or other empirical information. The theoretical developments in the current paper are pursued with this goal. Further, practical applications of LES demand the use of filters other than the Fourier cutoff filter chosen in previous OLES studies.[8–10] Therefore, the theory developed here is in the context of the finite-volume OLES described in Ref. 11. The development of the finite-volume formulation of OLES is recalled briefly below.

### A. Finite-volume optimal LES

In finite-volume OLES, the LES state variables are the velocities averaged over discrete volumes. The mapping (filter) is equivalent to the application of a top-hat filter followed by sampling on a grid. The LES evolution equations are then determined from the volume-averaged Navier–Stokes equations given by

$$V^v \frac{d\bar{u}_i^v}{dt} = -\sum_s \mathcal{F}_i^s - \sum_s \mathcal{P}_i^s + \sum_s \mathcal{V}_i^s, \tag{2}$$

where $\bar{u}_i^v$ is the velocity averaged over the volume $v$, $V^v$ is the volume of $v$, and $\mathcal{F}_i^s$, $\mathcal{P}_i^s$, and $\mathcal{V}_i^s$ are the convective flux, pressure force, and viscous flux, respectively, for the surface $s$. The sums in Eq. (2) are over the faces of the volume $v$. The quantities appearing in Eq. (2) are defined as

$$\bar{u}_i^v = \frac{1}{V^v}\int_v u_i d\mathbf{x}, \tag{3}$$

$$\mathcal{F}_i^s = \int_s u_i u_j n_j^s d\mathbf{x}, \tag{4}$$

$$\mathcal{P}_i^s = \int_s p n_i^s d\mathbf{x}, \tag{5}$$

$$\mathcal{V}_i^s = \int_s \nu \frac{\partial u_i}{\partial x_j} n_j^s d\mathbf{x}, \tag{6}$$

where $u_i$ is the turbulent velocity and $n_j^s$ is the outward-pointing unit normal to the surface $s$. As indicated, the integrals are over a volume $v$ or one of the faces $s$ bounding a volume. To distinguish the simulation quantities in a LES from the filtered real turbulence, the symbol $w_i^v$ will be used to represent the LES variables. The goal, of course, is for the dynamics and statistics of $w_i^v$ to approximate those of $\bar{u}_i^v$ as closely as possible.

The evolution equation for $w_i^v$ will be the same as that for $\bar{u}_i^v$ Eq. (2), with the fluxes replaced by models. In the context of OLES, the fluxes $\mathcal{F}_i^s$, $\mathcal{P}_i^s$, and $\mathcal{V}_i^s$ are to be modeled using stochastic estimation. For the current development, we will consider the limit of infinite Reynolds number in which the viscous flux $\mathcal{V}_i^s$ is negligible. Further, the pressure force will be treated as in Ref. 21 (see Sec. IV) so the development in this section will focus on the convective fluxes $\mathcal{F}_i^s$. These fluxes are to be modeled in terms of linear and quadratic functions of the LES state variables $w_i^v$. At least quadratic dependence is required here because the convective fluxes are themselves quadratic in the velocity. The estimate for the convective flux is thus of the form

$$\mathcal{F}_i^s \approx \mathcal{A}_i(s) + \sum_{v_1} \mathcal{L}_{ij}(s,v_1) w_j^{v_1} + \sum_{v_1,v_2} \mathcal{Q}_{ijk}(s,v_1,v_2) w_j^{v_1} w_k^{v_2}, \tag{7}$$

where $\mathcal{A}_i(s)$ is a constant term, $\mathcal{L}_{ij}(s,v)$ is the linear estimation kernel, and $\mathcal{Q}_{ijk}(s,v_1,v_2)$ is the quadratic estimation kernel. The range of the sums in Eq. (7) can be selected to be as large or small as desired, with the expectation that a larger range (a larger stencil) will produce more accurate results, though, as the stencil grows to include more distant and less well-correlated data, a diminishing return is expected.[8] It was found by Zandonade *et al.*[11] that a sum over four or six volumes was sufficient to get quite accurate LES results. In the LES performed here, a stencil is used that sums over four volumes (a $1\times1\times4$ stencil, see Ref. 11 and Sec. IV).

The minimum mean-square error between the ideal LES [Eq. (1)] and estimate [Eq. (7)] is attained when[8,10,17]

$$\langle \mathcal{F}_i^s \rangle = \mathcal{A}_i(s) + \sum_{v_1} \mathcal{L}_{ij}(s,v_1)\langle \bar{u}_j^{v_1}\rangle + \sum_{v_1,v_2} \mathcal{Q}_{ijk}(s,v_1,v_2)\langle \bar{u}_j^{v_1}\bar{u}_k^{v_2}\rangle, \tag{8}$$

$$\langle \mathcal{F}_i^s \bar{u}_l^{v_3}\rangle = \mathcal{A}_i(s)\langle \bar{u}_l^{v_3}\rangle + \sum_{v_1} \mathcal{L}_{ij}(s,v_1)\langle \bar{u}_j^{v_1}\bar{u}_l^{v_3}\rangle + \sum_{v_1,v_2} \mathcal{Q}_{ijk}(s,v_1,v_2)\langle \bar{u}_j^{v_1}\bar{u}_k^{v_2}\bar{u}_l^{v_3}\rangle, \tag{9}$$

$$\langle \mathcal{F}_i^s \bar{u}_l^{v_3}\bar{u}_m^{v_4}\rangle = \mathcal{A}_i(s)\langle \bar{u}_l^{v_3}\bar{u}_m^{v_4}\rangle + \sum_{v_1} \mathcal{L}_{ij}(s,v_1)\langle \bar{u}_j^{v_1}\bar{u}_l^{v_3}\bar{u}_m^{v_4}\rangle + \sum_{v_1,v_2} \mathcal{Q}_{ijk}(s,v_1,v_2)\langle \bar{u}_j^{v_1}\bar{u}_k^{v_2}\bar{u}_l^{v_3}\bar{u}_m^{v_4}\rangle. \tag{10}$$

These equations can be solved for the estimation coefficients (kernels) $\mathcal{A}_i$, $\mathcal{L}_{ij}$, and $\mathcal{Q}_{ijk}$. The statistical correlations appearing in the estimation equations (8)–(10) are needed as input for the OLES procedure. The theoretical determination of these correlations is the primary aim of this paper.

### B. Treatment of the mean

The estimation equations (7)–(10) apply directly regardless of the presence of a mean velocity. However, the correlations appearing in the equations, which must be provided as input, depend explicitly on the mean. This is inconvenient because we would like to model the correlations in a way that is applicable across a broad variety of turbulent flows. To accomplish this, the estimations need to be recast to separate out the dependence on the mean. To this end, we introduce a Reynolds decomposition of the velocities $u_i = U_i + u_i'$, $\bar{u}_i^v = \bar{U}_i^v + \bar{u}_i^{v\prime}$, and $w_i^v = W_i^v + w_i^{v\prime}$. The flux can then be decomposed as

$$\mathcal{F}_i^s = \mathcal{F}_i^{1s} + \mathcal{F}_i^{2s} + \mathcal{F}_i^{3s} + \mathcal{F}_i^{4s}, \tag{11}$$

with

$$\mathcal{F}_i^{1s} = \int_s U_i U_j n_j^s d\mathbf{x}, \tag{12}$$

$$\mathcal{F}_i^{2s} = \int_s U_i u_j' n_j^s d\mathbf{x}, \tag{13}$$

$$\mathcal{F}_i^{3s} = \int_s u_i' U_j n_j^s d\mathbf{x}, \tag{14}$$

$$\mathcal{F}_i^{4s} = \int_s u_i' u_j' n_j^s d\mathbf{x}. \tag{15}$$

Note, in particular, that $\langle \mathcal{F}_i^s \rangle = \mathcal{F}_i^{1s} + \langle \mathcal{F}_i^{4s}\rangle$. It is useful to consider the representation of each of these flux components separately. The primary flux of interest in this paper is $\mathcal{F}_i^{4s}$. A consistent OLES treatment of the other three fluxes is described in Appendix A.

The fluctuating flux $\mathcal{F}_i^{4s}$ is modeled as quadratic in the fluctuating velocity, resulting in model equations similar to Eqs. (7) and (10). In this case, when applied to $\mathcal{F}_i^{4s}$, they read

$$\mathcal{F}_i^{4s} \approx \mathcal{A}_i(s) + \sum_{v_1} \mathcal{L}_{ij}(s,v_1) w_j^{v_1'} + \sum_{v_1,v_2} \mathcal{Q}_{ijk}(s,v_1,v_2) w_j^{v_1'} w_k^{v_2'}, \tag{16}$$

$$\langle \mathcal{F}_i^{4s} \rangle = \mathcal{A}_i(s) + \sum_{v_1,v_2} \mathcal{Q}_{ijk}(s,v_1,v_2) \langle \bar{u}_j^{v_1'} \bar{u}_k^{v_2'} \rangle, \tag{17}$$

$$\langle \mathcal{F}_i^{4s} \bar{u}_l^{v_3'} \rangle = \sum_{v_1} \mathcal{L}_{ij}(s,v_1) \langle \bar{u}_j^{v_1'} \bar{u}_l^{v_3'} \rangle + \sum_{v_1,v_2} \mathcal{Q}_{ijk}(s,v_1,v_2) \langle \bar{u}_j^{v_1'} \bar{u}_k^{v_2'} \bar{u}_l^{v_3'} \rangle, \tag{18}$$

$$\langle \mathcal{F}_i^{4s} \bar{u}_l^{v_3'} \bar{u}_m^{v_4'} \rangle = \mathcal{A}_i(s) \langle \bar{u}_l^{v_3'} \bar{u}_m^{v_4'} \rangle + \sum_{v_1} \mathcal{L}_{ij}(s,v_1) \langle \bar{u}_j^{v_1'} \bar{u}_l^{v_3'} \bar{u}_m^{v_4'} \rangle + \sum_{v_1,v_2} \mathcal{Q}_{ijk}(s,v_1,v_2) \langle \bar{u}_j^{v_1'} \bar{u}_k^{v_2'} \bar{u}_l^{v_3'} \bar{u}_m^{v_4'} \rangle. \tag{19}$$

Given the correlations appearing in Eqs. (17)–(19), the kernels $\mathcal{A}_i$, $\mathcal{L}_{ij}$, and $\mathcal{Q}_{ijk}$ can be determined although it is important to note that they will not be the same as those obtained by solving Eqs. (8)–(10). Similarly, estimation kernels used in the formulation of $\mathcal{F}_i^{2s}$ and $\mathcal{F}_i^{3s}$ ($\mathcal{P}$ and $\mathcal{R}$, see Appendix A) can be determined given the required correlations in Eqs. (A7) and (A8). Finally, as explained in Appendix A, approximations for $\mathcal{F}_i^{1s}$ are obtained from standard numerical analysis considerations, completing the model for $\mathcal{F}_i^s$. The advantage of this divide-and-conquer approach is that the required correlations now involve only fluctuating velocities. In many turbulent flows, provided the filter scale is sufficiently small, and the inhomogeneities are not too strong (as near a wall), a reasonable modeling ansatz is that turbulence *fluctuations* on the scale of several filter widths (grid sizes) are homogeneous and isotropic.

We will use the isotropy assumption to model the correlations appearing in these estimation equations, which are inputs to the OLES procedure.[22] Zandonade *et al.*[11] obtained these correlations by processing DNS fields for isotropic turbulence. In Secs. III–V we see how they can be determined from theory and other considerations.

## III. THEORETICAL DETERMINATION OF CORRELATIONS

The correlations required for the OLES formulation are among the LES state variables (volume-averaged velocities) and the modeled quantities (convective fluxes). To determine them theoretically, they must be related to turbulence statistical quantities for which we have theories.

### A. LES correlations and multipoint velocity correlations

The correlations appearing in Eqs. (17)–(19), (A7), and (A8) and can be expressed as surface and volume integrals of multipoint velocity correlations. In particular, we have

$$\langle \mathcal{F}_i^{4s} \bar{u}_l^{v_3'} \rangle = I_{li}^1(v_3,s) = \frac{1}{v_3} \int_{v_3} \int_s \langle u_l'(\mathbf{x}^3) u_i'(\mathbf{x}) u_s'(\mathbf{x}) \rangle d\mathbf{x} d\mathbf{x}^3, \tag{20}$$

$$\langle \bar{u}_j^{v_1'} \bar{u}_l^{v_3'} \rangle = I_{lj}^2(v_3,v_1) = \frac{1}{v_3 v_1} \int_{v_3} \int_{v_1} \langle u_l'(\mathbf{x}^3) u_j'(\mathbf{x}^1) \rangle d\mathbf{x}^1 d\mathbf{x}^3, \tag{21}$$

$$\langle \bar{u}_j^{v_1'} \bar{u}_k^{v_2'} \bar{u}_l^{v_3'} \rangle = I_{ljk}^3(v_3,v_1,v_2) = \frac{1}{v_3 v_1 v_2} \int_{v_3} \int_{v_1} \int_{v_2} \langle u_l'(\mathbf{x}^3) u_j'(\mathbf{x}^1) u_k'(\mathbf{x}^2) \rangle d\mathbf{x}^2 d\mathbf{x}^1 d\mathbf{x}^3, \tag{22}$$

$$\langle \mathcal{F}_i^{4s} \bar{u}_l^{v_3'} \bar{u}_m^{v_4'} \rangle = I_{lmi}^4(v_3,v_4,s) = \frac{1}{v_3 v_4} \int_{v_3} \int_{v_4} \int_s \langle u_l'(\mathbf{x}^3) u_m'(\mathbf{x}^4) u_i'(\mathbf{x}) u_s'(\mathbf{x}) \rangle d\mathbf{x} d\mathbf{x}^4 d\mathbf{x}^3, \tag{23}$$

$$\langle \bar{u}_j^{v_1'} \bar{u}_k^{v_2'} \bar{u}_l^{v_3'} \bar{u}_m^{v_4'} \rangle = I_{lmjk}^5(v_3,v_4,v_1,v_2) = \frac{1}{v_3 v_4 v_1 v_2} \int_{v_3} \int_{v_4} \int_{v_1} \int_{v_2} \langle u_l'(\mathbf{x}^3) u_m'(\mathbf{x}^4) u_j'(\mathbf{x}^1) u_k'(\mathbf{x}^2) \rangle d\mathbf{x}^2 d\mathbf{x}^1 d\mathbf{x}^4 d\mathbf{x}^3, \tag{24}$$

$$\langle \tilde{u}_i' \bar{u}_k^{v_2\prime} \rangle = I_{ik}^6(v_2,s) = \frac{1}{v_2}\int_{v_2}\int_s \langle u_k'(\mathbf{x}^2)u_i'(\mathbf{x})\rangle d\mathbf{x}d\mathbf{x}^2, \quad (25)$$

$$\langle \tilde{u}_s' \bar{u}_k^{v_2\prime} \rangle = I_{sk}^7(v_2,s) = \frac{1}{v_2}\int_{v_2}\int_s \langle u_k'(\mathbf{x}^2)u_s'(\mathbf{x})\rangle d\mathbf{x}d\mathbf{x}^2. \quad (26)$$

In the above expressions, three correlation tensors are needed to determine the estimation coefficients. Models for these tensors must be provided as input to the OLES procedure. To develop these models, a number of assumptions will be made. First, it is assumed that on length scales required for the analysis (i.e., several filter widths), the turbulence is both homogeneous and isotropic. Using homogeneity, the required correlations are written as

$$\mathbb{R}_{ij}(\mathbf{r}^1) = \langle u_i'(\mathbf{x})u_j'(\mathbf{x}^1)\rangle, \quad (27)$$

$$\mathbb{T}_{ijk}(\mathbf{r}^1,\mathbf{r}^2) = \langle u_i'(\mathbf{x})u_j'(\mathbf{x}^1)u_k'(\mathbf{x}^2)\rangle, \quad (28)$$

$$\mathbb{F}_{ijkl}(\mathbf{r}^1,\mathbf{r}^2,\mathbf{r}^3) = \langle u_i'(\mathbf{x})u_j'(\mathbf{x}^1)u_k'(\mathbf{x}^2)u_l'(\mathbf{x}^3)\rangle, \quad (29)$$

with the dependence expressed in terms of spatial separations, $\mathbf{r}^i = \mathbf{x} - \mathbf{x}^i$.

Second, it is assumed that the spatial separations are small enough to be within the Kolmogorov inertial range and that the Reynolds number based on the filter width is sufficiently large that it can be considered to be infinite. With these assumptions, the Kolmogorov[23,24] expressions for the second- and third-order longitudinal structure functions are valid,

$$S_2(r) = \langle [u_\parallel(\mathbf{x}) - u_\parallel(\mathbf{x}^1)]^2\rangle = C\epsilon^{2/3}r^{2/3}, \quad (30)$$

$$S_3(r) = \langle [u_\parallel(\mathbf{x}) - u_\parallel(\mathbf{x}^1)]^3\rangle = -\frac{4}{5}\epsilon r, \quad (31)$$

where $r = |\mathbf{r}|$ is the magnitude of the separation vector, $u_\parallel$ is the velocity component in the direction of the separation vector, and $C$ is the Kolmogorov constant. From these expressions and isotropy and continuity constraints, expressions for the two-point second- and third-order correlations can be derived,

$$\mathbb{R}_{ij}(\mathbf{r}) = u^2\delta_{ij} + \frac{C}{6}\epsilon^{2/3}r^{-4/3}[r_i r_j - 4r^2\delta_{ij}], \quad (32)$$

$$\mathbb{T}_{ijk}(0,\mathbf{r}) = \frac{\epsilon}{15}\left[\delta_{ij}r_k - \frac{3}{2}(\delta_{ik}r_j + \delta_{jk}r_i)\right]. \quad (33)$$

The result for the second-order correlation is well known. The expression for the third-order correlation is less common but it is a direct consequence of the 4/5 law [Eq. (31)] and the general isotropic form derived by von Kármán and Howarth[25] (see also Refs. 26 and 27). Further, the analysis leading to Eq. (33) is implicit to the derivation of the 4/5 law. The two-point third-order correlation in Eq. (33) is precisely the correlation needed for the integral $I^1$ [Eq. (20)]. However, the more general third-order three-point correlation is needed for $I^3$ [Eq. (22)] (see below).

Finally, to determine an expression for $\mathbb{F}_{ijkl}$, we invoke the quasinormal approximation, which states that the fourth-order cumulants are zero. This implies that $\mathbb{F}$ can be expressed in terms of the two-point correlation $\mathbb{R}$,

$$\mathbb{F}_{ijkl}(\mathbf{r}^1,\mathbf{r}^2,\mathbf{r}^3) \approx \mathbb{R}_{ij}(\mathbf{r}^1)\mathbb{R}_{kl}(\mathbf{r}^3-\mathbf{r}^2) + \mathbb{R}_{ik}(\mathbf{r}^2)\mathbb{R}_{jl}(\mathbf{r}^3-\mathbf{r}^1) + \mathbb{R}_{il}(\mathbf{r}^3)\mathbb{R}_{jk}(\mathbf{r}^2-\mathbf{r}^1). \quad (34)$$

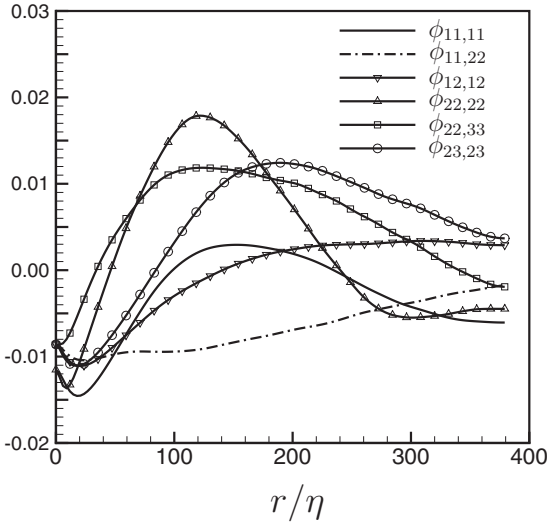


FIG. 1. Relative error $\phi_{ij,kl}$ in the quasinormal approximation to the nonzero elements of the fourth-order correlation $\mathbb{F}_{ijkl}(0,\mathbf{r},\mathbf{r})$, with separation in the $x_1$ direction. To obtain $\phi$, the error in $\mathbb{F}$ is normalized by $[\mathbb{F}_{ijkl}\mathbb{F}_{ijkl}(0,\mathbf{r},\mathbf{r})]^{1/2}$. Due to isotropy 2 and 3 indices can be swapped with identical results.

The quasinormal approximation is infamous in turbulence because it is well known to result in unrealizable spectra when used in two-point closure models.[28–31] However, its application here in OLES modeling can result in no such catastrophe because the LES equations being solved are not for statistical quantities to which realizability constraints apply. Similarly, the modifications added to the quasinormal approximation to assure realizability in two-point closures, such as "eddy damping" and Markovization in eddy-damped quasinormal Markovian,[31] are applied to the evolution equation for third-order correlations. Since no such correlation evolution equations are being solved here, these refinements are not applicable. Finally, the quasinormal approximation is generally quite accurate in isotropic turbulence.[32] For example, the error was measured in a forced isotropic turbulence DNS at $\mathrm{Re}_\lambda = 164$,[8] and is shown in Fig. 1. The small magnitude of these errors does not necessarily imply that they are dynamically insignificant. Ultimately, the performance of the resulting models is the most important measure of the accuracy of these approximations (see Sec. IV).

With the exception of the third-order three-point correlation needed to determine $I^3$, all the correlations required for the OLES model have now been defined. Unfortunately, the simple theories employed here are not sufficient to determine an expression for the three-point third-order correlation. Indeed, just writing down the most general isotropic form satisfying continuity constraints is difficult.[33] Based on this most general form, Chang and Moser[15] developed a model for $\mathbb{T}_{ijk}(\mathbf{r}^1,\mathbf{r}^2)$ for stationary, incompressible, homogeneous, isotropic turbulence for separations $\mathbf{r}^1$ and $\mathbf{r}^2$ in the inertial

range, and under the assumptions of small-scale isotropy and infinite Reynolds number. This model is algebraically very complex, with more than 758 terms so it will not be written here. Computer programs to evaluate the tensor numerically are available at http://turbulence.ices.utexas.edu.

As an alternative to the theory-based correlations described above, it may be possible to determine some of the correlations in Eqs. (20)–(24) dynamically during a LES. This may be possible because the correlations represented by $I^2$, $I^3$, and $I^5$ are correlations among volume-averaged velocities, which are precisely the LES state variables. Thus these correlations can be computed directly in a LES and, if needed, used to determine the models in that LES. This approach was not pursued here in favor of the theoretically determined correlations described above.

### B. Scaling

It is useful to scale the integrated correlations and the kernels that appear in the OLES analysis to be order one, as this provides insight into the importance of the various terms. Note, however, that there are two length scales in this analysis: the filter width $\Delta$ and the large turbulence length scale $u^3/\epsilon$. Thus, not all the quantities will be scaled consistently.

Based on the forms of the various approximations to the correlations, we define the following scaled quantities (dependencies and subscripts have been suppressed for simplicity of notation):

$$\tilde{I}^1 = \frac{I^1}{\epsilon\Delta^3}, \tag{35}$$

$$\tilde{I}^2 = \frac{I^2}{u^2}, \tag{36}$$

$$\tilde{I}^3 = \frac{I^3}{\epsilon\Delta}, \tag{37}$$

$$\tilde{I}^4 = \frac{I^4}{u^4\Delta^2}, \tag{38}$$

$$\tilde{I}^5 = \frac{I^5}{u^4}, \tag{39}$$

$$\tilde{I}^6 = \frac{I^6}{u^2\Delta^2}, \tag{40}$$

$$\tilde{I}^7 = \frac{I^7}{u^2\Delta^2}, \tag{41}$$

$$\tilde{\mathcal{A}} = \frac{\mathcal{A}}{u^2\Delta^2}, \tag{42}$$

$$\tilde{\mathcal{L}} = \frac{\mathcal{L}}{\epsilon^{1/3}\Delta^{7/3}}, \tag{43}$$

$$\tilde{\mathcal{Q}} = \frac{\mathcal{Q}}{\Delta^2}. \tag{44}$$

The scaling of $\mathcal{L}$ deserves some explanation. The linear term will account for energy transfer to the small scales in an inertial range. Asymptotically, for small $\Delta$, it should thus have inertial range scaling ($\Delta$ and $\epsilon$). With these definitions, the equations for $\mathcal{A}$, $\mathcal{L}$, and $\mathcal{Q}$ [Eqs. (17)–(19)] can be rewritten as

$$\delta_{in} = \tilde{\mathcal{A}}_i + \sum_{v_1,v_2} \tilde{\mathcal{Q}}_{ijk}(s,v_1,v_2)\tilde{I}^2_{jk}(v_1,v_2), \tag{45}$$

$$\tilde{I}^1_{li}(v_3,s) = \gamma^{-2/3}\sum_{v_1} \tilde{\mathcal{L}}_{ij}(s,v_1)\tilde{I}^2_{lj}(v_3,v_1) + \sum_{v_1,v_2} \tilde{\mathcal{Q}}_{ijk}(s,v_1,v_2)\tilde{I}^3_{ljk}(v_3,v_1,v_2), \tag{46}$$

$$\tilde{I}^4_{lmi}(v_3,v_4,s) = \tilde{\mathcal{A}}_i\tilde{I}^2_{lm}(v_3,v_4) + \gamma^{4/3}\sum_{v_1} \tilde{\mathcal{L}}_{ij}(s,v_1)\tilde{I}^3_{lmj}(v_3,v_4,v_1) + \sum_{v_1,v_2} \tilde{\mathcal{Q}}_{ijk}(s,v_1,v_2)\tilde{I}^5_{lmjk}(v_3,v_4,v_1,v_2), \tag{47}$$

where $\gamma = \Delta\epsilon/u^3$ is the generally small ratio of the filter scale to the large turbulence scale, and $\delta_{in}$ is the Kronecker delta, with $n$ signifying the component normal to the surface $s$. The $\gamma$-dependence of the scaled integrated correlations can be written explicitly as

$$\tilde{I}^1 = \tilde{I}^{10}, \tag{48}$$

$$\tilde{I}^2 = \tilde{I}^{20} + \gamma^{2/3}\tilde{I}^{21}, \tag{49}$$

$$\tilde{I}^3 = \tilde{I}^{30}, \tag{50}$$

$$\tilde{I}^4 = \tilde{I}^{40} + \gamma^{2/3}\tilde{I}^{41} + \gamma^{4/3}\tilde{I}^{42}, \tag{51}$$

$$\tilde{I}^5 = \tilde{I}^{50} + \gamma^{2/3}\tilde{I}^{51} + \gamma^{4/3}\tilde{I}^{52}, \tag{52}$$

where the $\tilde{I}^{\alpha\beta}$ are the components of $\tilde{I}^\alpha$ that are scaled by $\gamma^{2\beta/3}$. They depend only on the spatial configuration of the volumes and surfaces over which the integrals are performed, but not on $\gamma$. They can be determined easily from the expressions for the second- and fourth-order correlations, and are given in Appendix B for the particular $1\times1\times4$ stencil used in this paper.

Finally, for small $\gamma$, the estimation kernels $\tilde{\mathcal{A}}$, $\tilde{\mathcal{L}}$, and $\tilde{\mathcal{Q}}$ can be expanded in an asymptotic series in integer powers of $\gamma^{2/3}$, as follows:

$$\tilde{\mathcal{A}} = \tilde{\mathcal{A}}^0 + \gamma^{2/3}\tilde{\mathcal{A}}^1 + \gamma^{4/3}\tilde{\mathcal{A}}^2 + \cdots, \tag{53}$$

$$\tilde{\mathcal{L}} = \tilde{\mathcal{L}}^0 + \gamma^{2/3}\tilde{\mathcal{L}}^1 + \gamma^{4/3}\tilde{\mathcal{L}}^2 + \cdots, \tag{54}$$

$$\tilde{\mathcal{Q}} = \tilde{\mathcal{Q}}^0 + \gamma^{2/3}\tilde{\mathcal{Q}}^1 + \gamma^{4/3}\tilde{\mathcal{Q}}^2 + \cdots . \quad (55)$$

Equations (45)–(47) can then be solved asymptotically for an approximation to the kernels valid for small $\gamma$. The solution process for $\tilde{\mathcal{L}}^0$ and $\tilde{\mathcal{Q}}^0$ for the particular LES performed in this paper is described in Sec. IV B.

## IV. APPLICATION OF THEORETICAL OPTIMAL LES

To assess the validity of the theoretically determined correlations for use in OLES models, several of the simulations performed by Zandonade *et al.*[11] were repeated with the theoretically determined correlations in place of the DNS-determined correlations used by Zandonade *et al.* The details of these simulations are given briefly below.

The simulations were performed for forced isotropic turbulence, using a finite-volume OLES formulation like that described here and, in more detail, in Ref. 11. As described in Sec. II A, three fluxes need to be estimated: the convective flux $\mathcal{F}$, the pressure force $\mathcal{P}$, and the viscous flux $\mathcal{V}$. In these simulations, the viscous fluxes are zero, consistent with the infinite Reynolds number assumption used for the convective fluxes. As described by Langford and Moser[21] and as implemented by Zandonade *et al.*,[11] the pressure force is determined by imposing an approximate divergence-free constraint, which is consistent with the second-order staggered grid finite-volume divergence operator. This is an optimal representation of divergence,[21] which minimizes the expected error incurred by imposing an approximate divergence-free constraint.

The primary model to be considered here is that for the convective fluxes $\mathcal{F}$. The theoretical models described in Sec. III for the multipoint correlations were integrated numerically to determine $\tilde{I}^\alpha$ as defined in Eqs. (20)–(24). Each term is a high-dimensional quadrature (up to nine dimensional for $I^3$) in a hypercube of side $\Delta$. Adaptive quadrature[34] implemented in the routine DCUHRE (available online at http://portal.acm.org) was used to perform the quadrature with an error tolerance of $10^{-7}$.

The integrals need to be performed for each combination of volumes and surface in the stencil and for each velocity component in the stencil. The stencil used here is a $1\times1\times4$ simple stencil on a staggered grid, which is stencil S4 as described by Zandonade *et al.*[11] This stencil was selected because Zandonade *et al.* found that it is the smallest that yields good *a posteriori* results. Because the stencil is defined on a staggered grid, its definition is somewhat complicated and will be only briefly described here (see Appendix B in Ref. 11 for a complete description). First, the stencil is "simple," in the sense defined by Zandonade *et al.*,[11] which means that only the velocity components that occur in the flux integral equation (4) being estimated are used as events. Consider a cell surface through which a flux is to be estimated. Here and throughout, the normal to the surface is in the $n$-direction, while the tangential direction will be designated as $t$ (we will not generally need to distinguish between the two tangential grid directions $t_1$ and $t_2$). The flux of $n$-momentum $(\int_s u_n u_n d\mathbf{x})$ is estimated only in terms of $w_n$ velocities in neighboring cells, while the flux of $t$-momentum $(\int_s u_t u_n d\mathbf{x})$ is estimated in terms of products of $w_t$ and $w_n$. Second, in the staggered grid, each surface for which a flux is to be estimated is associated with the grid for one of the velocity components. The stencil for that velocity component includes the two cells on either side of the surface, lined up along the surface normal. When the tangential flux is being estimated, the cells for the normal velocity component in the stencil are offset due to the staggering. In this case, the two cells of the grid for the normal component that contain half the flux surface in their interior are used in the stencil. See Fig. 2 for the stencil geometries.

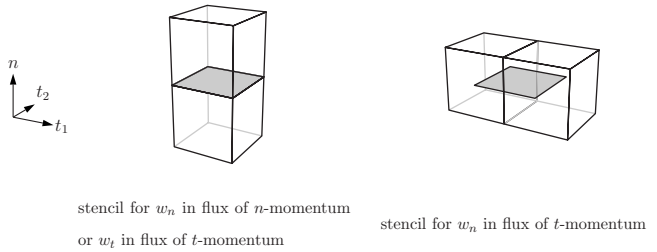


stencil for $w_n$ in flux of $n$-momentum or $w_t$ in flux of $t$-momentum

stencil for $w_n$ in flux of $t$-momentum

FIG. 2. Generic stencil geometries for the $1\times1\times2$ stencil on a staggered grid, for use when estimating fluxes on the faces shown in gray. The $1\times1\times4$ stencil used here is obtained by adding a cell above and below the stencil shown on the left (in the $n$ direction).

### A. Dynamic optimal LES

Since the advent of the dynamic procedure in LES modeling,[35] it has been a common practice to seek ways in which LES model parameters can be determined from the LES in which they are being used. This has the advantage of eliminating adjustable model constants and allowing the model to respond to the particular details of the flow. In the OLES models developed here, the constants in theoretical expressions (32) and (33) and in the model for $\mathbb{T}$ need to be determined. A total of seven constants are required: the velocity variance $u^2=2k/3$, the kinetic energy dissipation rate $\epsilon$, the Kolmogorov constant $C$, and four nondimensional constants in the model for $\mathbb{T}$.[15] The values of $u^2$ and $\epsilon$ are clearly flow dependent so dynamic considerations are particularly appropriate for these quantities. The Kolmogorov constant might be considered universal as Kolmogorov suggested, and in any case it is not expected to be strongly flow dependent. It could thus be given a fixed value $C\approx2$ (Ref. 16) or it could also be determined dynamically. Similarly, the four constants in the $\mathbb{T}$ model are also assumed to be flow independent so they can be given fixed values as Chang and Moser[15] did, or they can be determined dynamically.

Here we take the approach of only determining those quantities that are clearly flow dependent (i.e., $u^2$ and $\epsilon$), treating the other constants as universal. The Kolmogorov constant is given its usual value $C\approx2$ and the nondimensional constants in the model for $\mathbb{T}$ take the values used by Chang and Moser.[15] Setting these quantities directly reduces both the complexity of the simulations and the chance that the process of determining the constants will introduce spurious dynamics into the simulation.

Using the correlations derived previously (Sec. III) it is

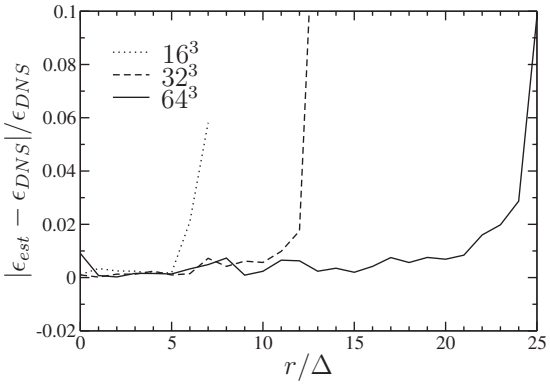


FIG. 3. Relative error in estimating the dissipation from the longitudinal third-order structure function of a finite-volume filtered velocity field using Eq. (57). Filtered structure functions were computed by filtering the DNS at $\mathrm{Re}_\lambda = 164$ of Ref. 8. The filter was defined on a cubical finite-volume grid of the size noted, on a periodic domain of size $2\pi$. Each finite volume is of size $\Delta$, and $r$ is the offset between the volumes used to compute the structure function.

straightforward to dynamically determine estimates of $u^2 = 2k/3$ and $\epsilon$ in a running LES. That is what is done here, with the values being set at each time step.

The longitudinal third-order structure function of the filtered (LES) turbulence can be expressed in terms of the dissipation, separation, mesh size, and $I^3$,

$$\bar{S}_3(v_1,v_2) = \langle(\bar{u}_1'(v_1) - \bar{u}_1'(v_2))^3\rangle = 6\Delta\epsilon\bar{I}^3_{111}(v_2,v_2,v_1), \tag{56}$$

where the volumes $v_1$ and $v_2$ are offset by a distance $r$ in the $x_1$ direction. The structure function $\bar{S}_3$ can be calculated from a LES field, allowing a consistent value of $\epsilon$ to be determined,

$$\epsilon = \frac{\langle(\bar{u}_1'(v_1) - \bar{u}_1'(v_2))^3\rangle}{6\Delta\tilde{I}^3_{111}(v_2,v_2,v_1)}. \tag{57}$$

The error in this dynamically determined value for the dissipation, $\epsilon_{\mathrm{est}}$, computed using filtered data from a DNS at $\mathrm{Re}_\lambda = 164$ (Ref. 8) is shown in Fig. 3. When the separation $r$ is in the inertial range, $\epsilon_{\mathrm{est}}$ is within a percent of the value determined directly from the DNS ($\epsilon_{\mathrm{DNS}}$).

The velocity variance can similarly be obtained from the statistics of filtered fields. The variance of the filtered velocity is simply

$$\langle(\bar{u}_1^{v_1\prime})^2\rangle = I^2_{11}(v_1,v_1) = u^2 + (\epsilon\Delta)^{2/3}\tilde{I}^{21}_{11}(v_1,v_1), \tag{58}$$

which, given $\epsilon$ from above and the variance of the filtered velocity, can be solved for $u^2$. This reconstruction of $u^2$ from filtered statistics was tested on the DNS discussed above, resulting in an error of less than 2%. Of course, the DNS is at finite Reynolds number so the infinite Reynolds number reconstruction will overestimate the value of $u^2$ in the DNS (or any finite Reynolds number flow). A finite Reynolds number correction can easily be formulated, by estimating the energy missing due to the viscous roll-off of the spectrum. The correction is proportional to $u^2/\mathrm{Re}_\lambda$, with a constant of proportionality of order one (the value depends on the assumed functional form of the viscous roll-off). For the DNS test discussed here, the correction is less than 1%.

One can also determine $u^2$ and $\epsilon$ in other ways. For example, they could be determined from the filtered two-point correlation evaluated with different separations. Here, $\epsilon$ was found using Eq. (57) because the third-order structure function is a direct measure of the transfer of energy between scales, and is thus more directly related to $\epsilon$. Further, using Eq. (57) allows $\epsilon$ to be determined independently of $u^2$, which will be convenient when using the asymptotic models (see Sec. IV B below) since in that case only $\epsilon$ needs to be estimated.

### B. Asymptotic optimal LES models

As mentioned in Sec. III B, the estimation equations (45)–(47) can be solved asymptotically for small $\gamma$. Use of the lowest order asymptotic kernels simplifies the LES model because it removes the $\gamma$ dependence of the kernels. Then, even when $u^2$ and $\epsilon$ are being determined dynamically, the scaled kernels do not change. Indeed, the lowest order quadratic kernel $\tilde{\mathcal{Q}}^0$ is scaled only with $\Delta$ so even when unscaled, the kernel only depends on the geometry of the cells being used to estimate the fluxes, and not $u^2$ and $\epsilon$. In this way, the asymptotic quadratic kernel can be thought of as a finite-volume scheme for the quadratic terms that is consistent with the statistics of turbulence. In addition to exploring the performance of theoretical OLES using the full kernels, determined without asymptotic approximation (the finite-$\gamma$ kernels), the performance of the lowest order asymptotic models will be evaluated.

The asymptotic solution for the kernels is easier to understand when applied to the simple optimal models employed here. Because of isotropy, we need only to consider the velocity component normal to the face through which the flux is being estimated and a generic velocity component tangential to the face being considered. In what follows, these components will be denoted with subscripts $n$ and $t$, respectively (repeated $n$ and $t$ do not imply summation). For simple OLES models, flux of normal momentum is estimated in terms of quadratic products of the form $u_n u_n$ and linear dependence on $u_n$ only. Tangential fluxes are estimated with quadratic and linear terms of the form $u_n u_t$ and $u_t$, respectively. As a consequence, the only quadratic kernel elements are $\tilde{\mathcal{Q}}_{nnn}$ and $\tilde{\mathcal{Q}}_{tnt}$, and the linear kernel elements are $\tilde{\mathcal{L}}_{\alpha\alpha}$, where the subscript $\alpha$ can be either $n$ or $t$, and no summation is implied.

When the asymptotic expansions of the kernels and matrices are substituted into the scaled estimation equations (45)–(47), one finds that the equation for $\tilde{\mathcal{Q}}^0$ derived from Eqs. (47) and (45) at zeroth order is singular because $I^{50}_{nnnn} = 3$, $I^{50}_{ntnt} = 1$, $I^{20}_{\alpha\alpha} = 1$, and $I^{20}_{nt} = 0$ regardless of the volumes being considered. Fortunately, the equations satisfy the solvability constraint so solutions exist. However, to find a unique solution, the solvability of Eqs. (47) and (45) at higher order must be considered. The equation (for the normal fluxes) at next order involves the

matrix $\tilde{I}^{Q1}_{nnnn}(v_3,v_4,v_1,v_2)=\tilde{I}^{51}_{nnnn}(v_3,v_4,v_1,v_2)-\tilde{I}^{21}_{nn}(v_3,v_4)-\tilde{I}^{21}_{nn}(v_1,v_2)$, which is also singular because it can easily be shown that

$$\tilde{I}^{Q1}_{nnnn}(v_3,v_4,v_1,v_2) = \tfrac{1}{2}[\tilde{I}^{Q1}_{nnnn}(v_3,v_3,v_1,v_2)+I^{Q1}_{nnnn}(v_4,v_4,v_1,v_2)]. \quad (59)$$

The right hand side of the equation at order $\gamma^{2/3}$ is in the column space of $\tilde{I}^{Q1}_{nnnn}$ because the structure of $\tilde{I}^{41}_{nnn}$ is such that

$$\tilde{I}^{41}_{nnn}(v_3,v_4,s)-\tilde{I}^{21}_{nn}(v_3,v_4) = \tfrac{1}{2}[\tilde{I}^{41}_{nnn}(v_3,v_3,s)+\tilde{I}^{41}_{nnn}(v_4,v_4,s) - \tilde{I}^{21}_{nn}(v_3,v_3)-\tilde{I}^{21}_{nn}(v_4,v_4)] \quad (60)$$

so solutions exist. To obtain a unique solution, the next order ($\gamma^{4/3}$) equation for $\tilde{\mathcal{Q}}_{nnn}$ must be considered. For the tangential flux operators, the equations at the next order involve the matrix $\tilde{I}^{51}_{ntnt}$, which is not singular for the stencil considered here. For larger stencils involving more volumes for the normal velocity component, $\tilde{I}^{51}_{ntnt}$ is singular, requiring that the order $\gamma^{4/3}$ equation be considered, as discussed above. Finally, Eq. (46) for $\tilde{\mathcal{L}}^0$ at order $\gamma^{-2/3}$ is also singular so the $\gamma^0$ equation must be considered to determine a unique solution. Actually, the ranks of the matrices in the lowest order equations for $\tilde{\mathcal{Q}}$ and $\tilde{\mathcal{L}}$ are each 2, and the rank of the next order equation in $\tilde{\mathcal{Q}}_{nnn}$ is the length of the stencil (4 for the $1\times1\times4$ stencil used here) so the higher order equations provide most of the information about the asymptotic kernels.

By using the known properties of $\tilde{I}^{50}$, $\tilde{I}^{Q1}_{nnnn}$, and $\tilde{I}^{20}_{\alpha\alpha}$ described above, the system of equations that must be solved for $\tilde{\mathcal{Q}}^0$ and $\tilde{\mathcal{L}}^0$ on the stencils used here can be simplified, with the result

$$\sum_{v_1,v_2}\tilde{\mathcal{Q}}^0_{nnn}(s,v_1,v_2)=1, \quad (61)$$

$$\sum_{v_1,v_2}\tilde{I}^{Q1}_{nnnn}(v_\beta,v_\beta,v_1,v_2)\tilde{\mathcal{Q}}^0_{nnn}(s,v_1,v_2) = \tilde{I}^{41}_{nnn}(v_\beta,v_\beta,s)-\tilde{I}^{21}_{nn}(v_\beta,v_\beta)+C_n, \quad (62)$$

$$\sum_{v_1,v_2}\tilde{I}^{Q2}_{nnnn}(v_3,v_4,v_1,v_2)\tilde{\mathcal{Q}}^0_{nnn}(s,v_1,v_2) = \tilde{I}^{42}_{nnn}(v_3,v_4,s)-\sum_{v_1}\tilde{\mathcal{L}}^0_{nn}(s,v_1)\tilde{I}^{3}_{nnn}(v_3,v_4,v_1) + \sum_\beta\frac{C_\beta}{2}(\delta_{v_\beta v_3}+\delta_{v_\beta v_4}), \quad (63)$$

$$\sum_{v_1,v_2}\tilde{\mathcal{Q}}_{tnt}(s,v_1,v_2)=1, \quad (64)$$

$$\sum_{v_1,v_2}\tilde{I}^{51}_{ntnt}(v_3,v_4,v_1,v_2)\tilde{\mathcal{Q}}^0_{tnt}(s,v_1,v_2)=\tilde{I}^{41}_{ntt}(v_3,v_4,s)+C_t, \quad (65)$$

TABLE I. Values of the elements of $\tilde{\mathcal{L}}^0$ as determined for the $1\times1\times4$ stencil, with volume labels as defined in Fig. 4. The value of $\tilde{\mathcal{L}}^0$ for volumes not listed here are determined from the symmetry $\tilde{\mathcal{L}}^0_{\alpha\alpha}(s,-v_1)=-\tilde{\mathcal{L}}^0_{\alpha\alpha}(s,v_1)$.

| $v_1$ | $\tilde{\mathcal{L}}^0_{nn}(s,v_1)$ | $\tilde{\mathcal{L}}^0_{tt}(s,v_1)$ |
|---|---|---|
| 2 | 0.057 64 | 0.026 23 |
| 1 | −0.390 59 | −0.127 68 |

$$\sum_{v_1}\tilde{\mathcal{L}}^0_{\alpha\alpha}(s,v_1)=0, \quad (66)$$

$$\sum_{v_1}\tilde{I}^{21}_{\alpha\alpha}(v_3,v_1)\tilde{\mathcal{L}}^0_{\alpha\alpha}(s,v_1) = \tilde{I}^{1}_{\alpha\alpha}(v_3,s)-\sum_{v_1,v_2}\tilde{\mathcal{Q}}^0_{\alpha n\alpha}(s,v_1,v_2)\tilde{I}^{3}_{\alpha n\alpha}(v_3,v_1,v_2)+C_\alpha, \quad (67)$$

where $\delta_{v_\beta v_i}$ is zero unless $v_\beta=v_i$, in which case it is one, and the constants $C_n$, $C_t$, $C_\beta$, and $C_\alpha$ must be solved for as part of the solution process. They provide the extra degrees of freedom required to allow Eqs. (61), (62), (64), and (66) to be satisfied, but are otherwise irrelevant to the current analysis. They are related to the next order term in the expansion for the kernels. The matrix $\tilde{I}^{Q2}$ is given by $\tilde{I}^{Q2}_{nnnn}(v_3,v_4,v_1,v_2)=\tilde{I}^{52}_{nnnn}(v_3,v_4,v_1,v_2)-\tilde{I}^{21}_{nn}(v_3,v_4)\tilde{I}^{21}_{nn}(v_1,v_2)$. Here and in Eq. (62) the volumes $v_\beta$ range over the stencil volumes.

Values of the scaled asymptotic kernel elements computed in this way are given in Tables I and II for the $1\times1\times4$ stencil. In these tables, the volume labels are as defined in Fig. 4, for estimates of the flux through the cell face between volumes $-1$ and 1.

The relative error incurred by using $\mathcal{Q}^0$ and $\mathcal{L}^0$ at finite $\gamma$ is of interest and can be measured as $e_Q=\|\mathcal{Q}-\mathcal{Q}^0\|/\|\mathcal{Q}\|$ and $e_L=\|\mathcal{L}-\mathcal{L}^0\|/\|\mathcal{L}\|$, where $\|\cdot\|$ is the $L^2$ matrix norm. As is clear from Fig. 5, for small $\gamma$, the errors $e_Q$ and $e_L$ go to zero like

TABLE II. Values of the elements of $\tilde{\mathcal{Q}}^0$ as determined for the $1\times1\times4$ stencil, with volume labels as defined in Fig. 4. The value of $\tilde{\mathcal{L}}^0$ for volumes not listed here are determined from the symmetry $\tilde{\mathcal{Q}}^0_{\alpha n\alpha}(s,-v_1,-v_2)=\tilde{\mathcal{Q}}^0_{\alpha n\alpha}(s,v_1,v_2)$.

| $v_1$ | $v_2$ | $\tilde{\mathcal{Q}}^0_{nnn}(s,v_1,v_2)$ |
|---|---|---|
| 2 | 2 | 0.009 13 |
| 2 | 1 | −0.114 85 |
| 2 | −1 | −0.214 32 |
| 2 | −2 | 0.043 86 |
| 1 | 1 | 0.214 67 |
| 1 | −1 | 1.16 690 |

| $v_1$ | $v_2$ | $\tilde{\mathcal{Q}}^0_{tnt}(s,v_1,v_2)$ |
|---|---|---|
| 0 | 2 | −0.066 17 |
| 0 | 1 | 0.316 17 |

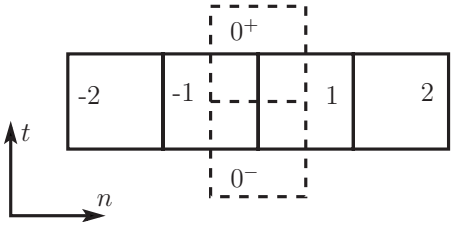


FIG. 4. Volumes (and their numbering) in a $1\times1\times4$ staggered grid stencil to estimate the flux through the surface between volumes $-1$ and 1. For the normal component flux ($n$), the volumes with solid outlines are on the $n$-component mesh, and the dashed-outline volumes are not used. For the tangential-component flux ($t$), the solid volumes are on the $t$-component mesh, and the dashed volumes are on the $n$-component mesh. In Tables I, II, and V–VIII, the volumes are referred to by the numbers shown here, but no distinction is made between $0^+$ and $0^-$ because the values associated with these volumes are the same.

$\gamma^{2/3}$. This asymptotic behavior is attained by $\gamma\approx0.1$, where the relative error ranges from 0.3% to 6%. Thus, it is expected that for $\gamma<0.1$ the asymptotic kernels will yield good LES simulations. The results of performing a LES with the asymptotic kernels are compared to that for the finite-$\gamma$ kernels in Sec. IV C.

### C. LES results

The performance of the theory-based OLES models developed here is evaluated in isotropic turbulence at infinite Reynolds number, simulated in a periodic cube with sides of length $L=2\pi$. The three dimensional energy spectra and third-order structure function obtained using a $1\times1\times4$ stencil[11] on a staggered grid are shown in Fig. 6 for different grid resolutions ($16^3$–$128^3$) corresponding to finite-volume filter widths varying from $\Delta\approx0.39$ to 0.05. In these forced isotropic turbulence simulations, the energy is injected at the rate $\epsilon\approx62.3468$, and the simulations result in a $u^2\approx28$, yielding $\gamma\approx0.17$–$0.02$ for the $16^3$–$128^3$ grid sizes, respectively. In all the spectra presented here, the wavenumber $k$ is normalized by $k_{\min}=2\pi/L$, and the three dimensional energy spectrum $E(k)$ is normalized by $\epsilon^{2/3}k_{\min}^{-5/3}$.

For all filter widths, the high wavenumber portion of the LES energy spectrum exhibits a slope consistent with the filtering of a $k^{-5/3}$ inertial range. For larger grid sizes and at lower wavenumbers, the shallower $k^{-5/3}$ slope is evident, and this range becomes longer with increased resolution. This is the converged, resolution-independent part of the solution. The shifting of the filtered part of the spectrum to higher wavenumbers with increasing resolution is expected since the filter width is being decreased. Similarly, the third-order longitudinal structure function agrees very closely with the theoretical filtered structure function obtained by integrating the third-order three-point correlation model[15] over the finite volumes. As expected, as the resolution increases, the simulation structure functions approach the $-\frac{4}{5}\epsilon r$ dependence expected in the inertial range. This suggests that LES is correctly representing the inertial range energy transfer. In short, the behavior exhibited in Fig. 6 is precisely what is expected, indicating that the theory-based OLES model is representing the effects of the unresolved scales at infinite Reynolds number in a consistent, resolution independent way.

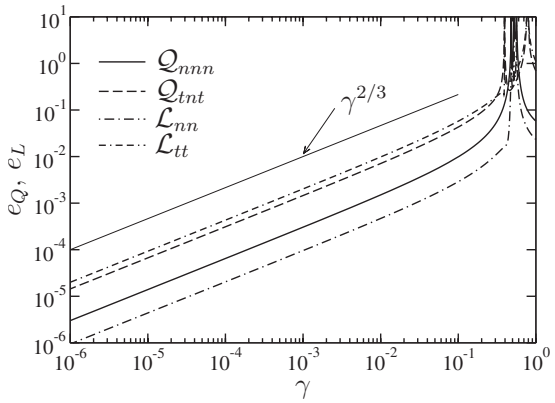


FIG. 5. The $L^2$ matrix norms $e_Q$ and $e_L$ of the difference between the asymptotic $1\times1\times4$ kernels and the kernels at finite $\gamma$, as a function of $\gamma$.

The LES results presented in Fig. 6 were obtained using the finite-$\gamma$ OLES kernels, but as indicated in Sec. IV B, it will generally be more convenient to use the small-$\gamma$ asymptotic kernels. A comparison of LES results from the finite-$\gamma$ and asymptotic kernels is shown in Fig. 7. At both $128^3$ and $32^3$ resolutions, corresponding to $\gamma\approx0.02$ and 0.08, respectively, the spectra and structure functions from the two cases are indistinguishable.

A finite Reynolds number case was simulated using OLES to gauge the performance of the optimal models compared to a standard model (dynamic Smagorinsky). Spectra and structure functions from these simulations are shown in Fig. 8 along with that from filtered DNS. Results for both $1\times1\times2$ and $1\times1\times4$ stencils on a staggered $32^3$ grid are shown. With the dynamic Smagorinsky model, the two stencils correspond to second- and fourth-order schemes. Comparing the $1\times1\times4$ stencil optimal model to the corresponding dynamic model, a sharp roll-off of the spectrum at high wavenumbers is evident with the dynamic model, but not present in the optimal model. The optimal model apparently yields a better treatment of the model dissipation at high wavenumbers. However, the $1\times1\times2$ stencil optimal model does have the sharp roll-off. The optimal model spectra also have a somewhat steeper slope than either the filtered DNS or the dynamic model, but this slope is consistent with the filtered $k^{-5/3}$ spectrum. Optimal models for these stencils that are based on the DNS correlations do not exhibit this difference in slope of the spectrum between the model and filtered DNS (see Ref. 11). It appears that the optimal model results reflect the infinite Reynolds number theory on which the correlations are based, which is not strictly applicable to this moderate Reynolds number case. For the third-order structure function, the optimal models are somewhat more accurate in the midrange of separations than the dynamic Smagorinsky. Otherwise, the model results are comparable.

At high Reynolds numbers these optimal models should yield accurate results (as seen in Fig. 6), and will generally be superior to the dynamic model due to the elimination of the sharp spectral roll-off near the cutoff.

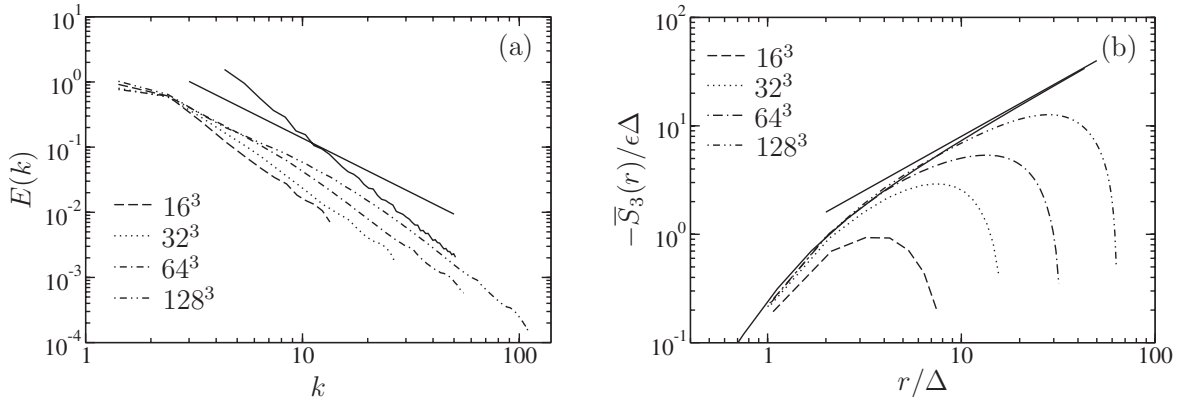


FIG. 6. Three-dimensional energy spectra (a) and third-order structure functions (b) from OLES of isotropic turbulence at infinite Reynolds number using the finite-$\gamma$ kernels, with resolutions ranging from $16^3$ to $128^3$ ($\gamma \approx 0.17$ to $\gamma \approx 0.02$, respectively). The solid lines in both plots are determined from the Kolmogorov theory. In (a), the two solid lines are a $k^{-5/3}$ slope (shallow), and the result of filtering a $k^{-5/3}$ spectrum. In (b) the straight line is $S_3 = -\frac{4}{5}\epsilon r$, and the other solid line is the structure function of the filtered velocity determined from $I^3$.

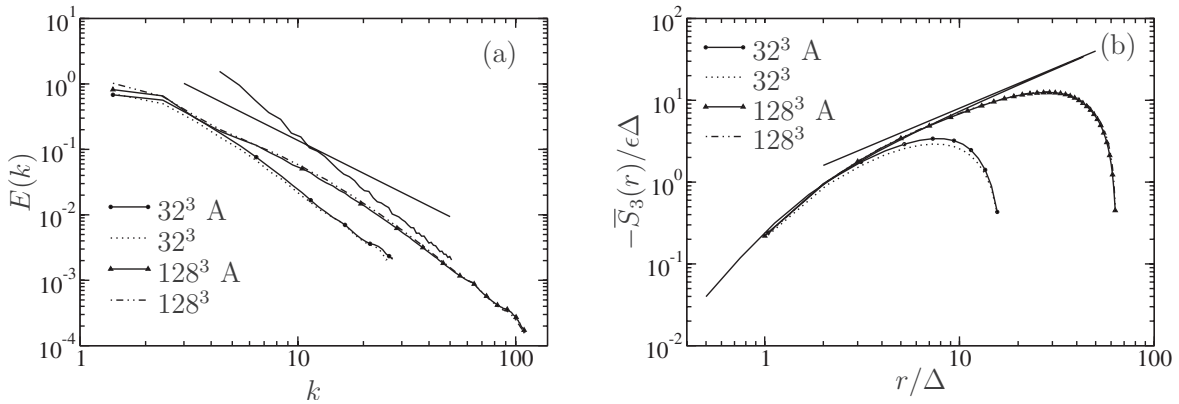


FIG. 7. Three-dimensional energy spectra (a) and third-order structure functions (b) from OLES of isotropic turbulence at infinite Reynolds number using both finite $\gamma$ and asymptotic kernels (signified with "A"), with resolution $32^3$ and $128^3$ ($\gamma = 0.08$ and $\gamma = 0.02$, respectively). Solid lines in (a) and (b) are as in Fig. 6.

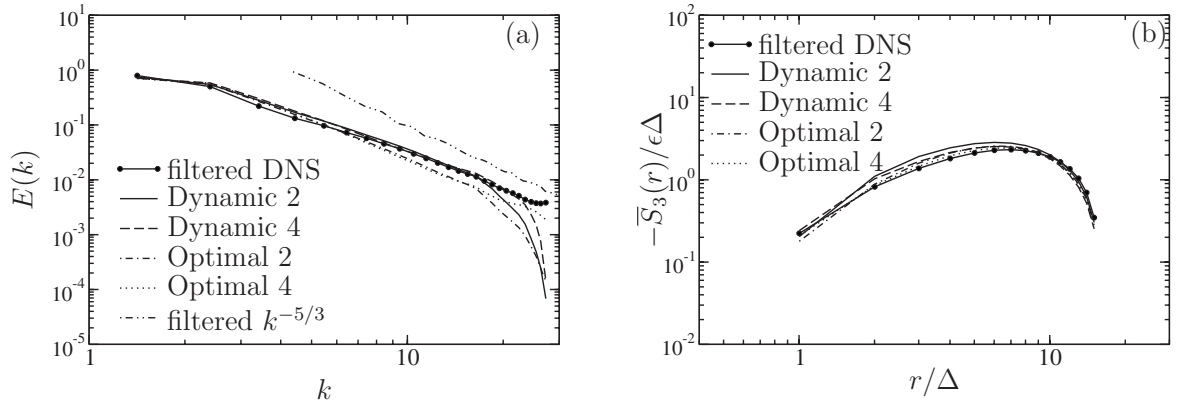


FIG. 8. Three-dimensional energy spectra (a) and third-order structure function (b) from LES of isotropic turbulence on a $32^3$ finite-volume grid at $\mathrm{Re}_\lambda = 164$ using the dynamic Smagorinsky model and finite-$\gamma$ optimal models, with $1 \times 1 \times 2$ and $1 \times 1 \times 4$ stencils. Also shown is a filtered DNS. Numbers on the curve labels indicate the stencil size, 2 signifies the $1 \times 1 \times 2$ stencil, and 4 is the $1 \times 1 \times 4$ stencil.

## V. CHARACTERIZATION OF THE ASYMPTOTIC KERNELS

The results of Sec. IV show that the OLES models and, in particular, the asymptotic $\gamma \to 0$ models perform remarkably well. It is useful, then, to analyze the character of the quadratic and linear kernels that make up these models.

The OLES kernels model the convective flux of momentum through the faces of each finite-volume cell in the LES representation. As such, the kernels replace the approximation of the convective terms in a standard finite-volume scheme so as to account for the presence of small-scale turbulence. In particular, the asymptotic kernels can be thought of as a finite-volume scheme representing infinite Reynolds number turbulence. Here we consider the numerical characteristics of these kernels, as compared to standard finite-volume approximations. The differences in the kernels account for the difference between a LES and a well-resolved simulation, including subgrid effects.

### A. Operator contributions to energy transfer

To analyze the operators, we need to consider the difference in the convective fluxes through cell faces on opposite sides of a cell, as this is what appears in the evolution equation for the cell averaged velocity. The resulting operators for the velocity components normal and tangential to the face are different and are given by

$$\mathcal{F}_n^+ - \mathcal{F}_n^- = \sum_{v_1^n v_2^n} \mathcal{Q}_{nnn}(v_1^n, v_2^n)(w_n^{v_1^n} w_n^{v_2^n} - w_n^{v_1^n - 1} w_n^{v_2^n - 1}) + \sum_{v^n} \mathcal{L}_{nn}(v^n)(w_n^{v^n} - w_n^{v^n - 1}), \tag{68}$$

$$\mathcal{F}_t^+ - \mathcal{F}_t^- = \sum_{v^n v^t} \mathcal{Q}_{tnt}(v^n, v^t)(w_n^{v^n} w_t^{v^t} - w_n^{v^n - 1} w_t^{v^t - 1}) + \sum_{v^t} \mathcal{L}_{tt}(v^t)(w_t^{v^t} - w_t^{v^t - 1}), \tag{69}$$

where the volume $v-1$ is the neighbor of volume $v$ in the negative $n$ direction.

In the commonly used Harlow–Welch staggered grid scheme,[36] the approximation of the nonlinear terms is energy conserving, preserving the analytic character of the terms in the Navier–Stokes equations. However, in these LES models for infinite Reynolds number turbulence, the model of the convective fluxes must represent the transfer of energy to the unresolved turbulence so the models cannot be energy conserving. The expected value of the energy transfer rate can be easily determined from the kernels and the $I^2$ and $I^3$ integrals by evaluating *a priori* $\langle w^{v_0^\alpha}(\mathcal{F}_\alpha^+ - \mathcal{F}_\alpha^-)\rangle / \Delta^3$, where $\alpha$ is either $n$ or $t$, and $v_0^\alpha$ is the volume for which the fluxes are computed. The contribution of the quadratic and linear terms in the normal and tangential equations is thus given by

$$\epsilon_n^{\mathcal{Q}} = \epsilon \sum_{v_1^n, v_2^n} \widetilde{\mathcal{Q}}_{nnn}(v_1^n, v_2^n)[\widetilde{I}^3_{nnn}(v_0^n, v_1^n, v_2^n) - \widetilde{I}^3_{nnn}(v_0^n, v_1^n - 1, v_2^n - 1)], \tag{70}$$

TABLE III. Contributions to dissipation of the quadratic ($\epsilon^{\mathcal{Q}}$) and linear ($\epsilon^{\mathcal{L}}$) portions of the asymptotic LES operators for flux of the normal momentum (normal) and tangential momentum (tangential). The sum $3N+6T$ signifies three times the normal contribution plus six times the tangential, which represents the contributions to the total dissipation of kinetic energy ($\epsilon$).

| Operator | $\epsilon^{\mathcal{Q}}/\epsilon$ | $\epsilon^{\mathcal{L}}/\epsilon$ | $(\epsilon^{\mathcal{Q}}+\epsilon^{\mathcal{L}})/\epsilon$ |
|---|---|---|---|
| Normal | 0.027 097 | −0.160 430 | −0.133 333 |
| Tangential | −0.010 070 | −0.089 930 | −0.100 000 |
| $3N+6T$ | 0.020 870 | −1.020 870 | −1.000 000 |

$$\epsilon_n^{\mathcal{L}} = \epsilon \sum_{v^n} \widetilde{\mathcal{L}}_{nn}(v^n)[\widetilde{I}^2_{nn}(v_0^n, v^n) - \widetilde{I}^2_{nn}(v_0^n, v^n - 1)], \tag{71}$$

$$\epsilon_t^{\mathcal{Q}} = \epsilon \sum_{v^t, v^n} \widetilde{\mathcal{Q}}_{tnt}(v_1^n, v_2^n)[\widetilde{I}^3_{tnt}(v_0^t, v^n, v^t) - \widetilde{I}^3_{tnt}(v_0^t, v^n - 1, v^t - 1)], \tag{72}$$

$$\epsilon_t^{\mathcal{L}} = \epsilon \sum_{v^t} \widetilde{\mathcal{L}}_{tt}(v^t)[\widetilde{I}^2_{tt}(v_0^t, v^t) - \widetilde{I}^2_{tt}(v_0^t, v^t - 1)]. \tag{73}$$

The net contribution of the quadratic and linear terms in the model for the flux of normal and tangential momentum to energy transfer is given in Table III. Also the total transfer to small scales is given by $3(\epsilon_n^{\mathcal{Q}} + \epsilon_n^{\mathcal{L}}) + 6(\epsilon_t^{\mathcal{Q}} + \epsilon_t^{\mathcal{L}})$ to account for the three spatial directions and the two independent tangential directions. Note that the quadratic term does not, on average, dissipate kinetic energy, but instead produces it. The linear term is sufficiently dissipative to make up for this production, and to dissipate at the required rate ($\epsilon$). Furthermore, the spectra of the linear operators (discussed below and in Fig. 9) show that they are negative definite so that they dissipate everywhere in space. However, it is possible for the quadratic term to locally generate energy at a rate

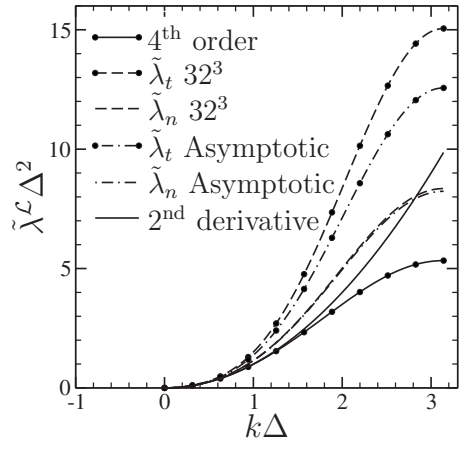


FIG. 9. Spectra $\lambda^{\mathcal{L}}$ of the linear operators. Spectra have been scaled so that they are consistent approximations to the (negative) second derivative. Shown are the spectra for the asymptotic operators ($\gamma=0$) and those determined for a $32^3$ grid ($\gamma=0.08$). $\lambda_t$ and $\lambda_n$ are the spectra for the $\widetilde{\mathcal{L}}^0_{tt}$ and $\widetilde{\mathcal{L}}^0_{nn}$ operators, respectively. Note that these operators are formulated to represent the flux $\mathcal{F}^{\mathcal{S}}$ in Eq. (2), which appear with a minus sign so a positive $\lambda^{\mathcal{L}}$ is dissipative.

higher than the local dissipation by the linear term, which could represent backscatter. Perhaps this is a part of the reason that the nonlinear operator is antidissipative.

### B. Spectral analysis of the operators

Another way to characterize the operators is to examine their spectrum, by considering their action on velocity fields given by $w_j = e^{ijk\Delta}$, where $j$ is a cell index that increments in the $n$ direction, $k$ is a wavenumber, and here $i=\sqrt{-1}$. This is, of course, relevant because a general filtered variable $w_j$ can be written as the sum of such Fourier modes. For the linear parts of the operator the (normalized) spectrum $\tilde{\lambda}^{\mathcal{L}}(k)$ is given by

$$\tilde{\lambda}_n^{\mathcal{L}}(k) = \sum_j \tilde{\mathcal{L}}_{nn}(v_0^n, v_0^n + j)(e^{ijk\Delta} - e^{i(j-1)k\Delta}), \tag{74}$$

$$\tilde{\lambda}_t^{\mathcal{L}}(k) = \sum_j \tilde{\mathcal{L}}_{tt}(v_0^t, v_0^t + j)(e^{ijk\Delta} - e^{i(j-1)k\Delta}). \tag{75}$$

The symmetry properties of $\tilde{\mathcal{L}}$ imply that the $\tilde{\lambda}^{\mathcal{L}}$ are real and, as defined here, positive $\tilde{\lambda}^{\mathcal{L}}(k)$ implies that the term is dissipative at wavenumber $k$. Further, the symmetry properties and the way the $\mathcal{L}$ operator enters the equations as the difference between opposite faces implies that the $\tilde{\mathcal{L}}$ operator is a second-order approximation to the second derivative times a constant. The $\lambda^{\mathcal{L}}$ are plotted in Fig. 9 along with the spectrum of a five-point fourth-order approximation of the (negative) second derivative, which has the same stencil width. The $\tilde{\mathcal{L}}$ spectra have been normalized to be consistent with a representation of the second derivative. It is clear that $\tilde{\mathcal{L}}_{tt}^0$ is more dissipative at high wavenumbers than would be the case for the second derivative operator, or its fourth-order approximation, while the $\tilde{\mathcal{L}}_{nn}^0$ operator is about as dissipative at high wavenumbers as the second derivative. The operators determined for our $32^3$ case ($\gamma=0.08$) are similar to the asymptotic operators ($\gamma=0$), although $\tilde{\mathcal{L}}_{tt}$ is more dissipative at high wavenumbers for the $32^3$ operators.

When the quadratic operators are applied to filtered variables expressed as sums of Fourier modes, the result is the sum of all the cross terms in which the operator is acting bilinearly on Fourier functions $w_j = e^{ijk\Delta}$ and $\tilde{w}_l = e^{il\tilde{k}\Delta}$ with different wave numbers $k$ and $\tilde{k}$. The relevant spectra are thus the bilinear spectra $\tilde{\lambda}^{\mathcal{Q}}(k,\tilde{k})$ given by

$$\tilde{\lambda}_n^{\mathcal{Q}}(k,\tilde{k}) = \sum_{j,l} \tilde{\mathcal{Q}}_{nnn}(v_0^n, v_0^n + j, v_0^n + l) \times (e^{ijk\Delta} e^{il\tilde{k}\Delta} - e^{i(j-1)k\Delta} e^{i(l-1)\tilde{k}\Delta}), \tag{76}$$

$$\tilde{\lambda}_t^{\mathcal{Q}}(k,\tilde{k}) = \sum_{l,v_0^n} \tilde{\mathcal{Q}}_{tnt}(v_0^t, v^n, v_0^t + l) \times (e^{ik\Delta/2} e^{il\tilde{k}\Delta} - e^{-ik\Delta/2} e^{i(l-1)\tilde{k}\Delta}), \tag{77}$$

where we have used the fact that for the stencils considered here $\tilde{\mathcal{Q}}_{tnt}$ only involves normal component volumes $v^n$ that are offset by $\pm\Delta/2$ from $v_0^t$. Because of the symmetries in $\tilde{\mathcal{Q}}$, the $\tilde{\lambda}^{\mathcal{Q}}$ are pure imaginary. Contours of these bilinear spectra are shown in Fig. 10 for the $32^3$ operators, the asymptotic operators, and a fourth-order approximation to $\partial w\tilde{w}/\partial n$ that can be formulated on the same stencil (products of the fourth-order interpolation of the filtered velocity to the flux surface). Note that because of constraints (61) and (64) on $\tilde{\mathcal{Q}}_{nnn}$ and $\tilde{\mathcal{Q}}_{tnt}$, they are consistent second-order approximations to $\partial w_n\tilde{w}_n/\partial n$ and $\partial w_n\tilde{w}_t/\partial n$, respectively.

For both the normal and tangential $\tilde{\mathcal{Q}}$ operators, the $32^3$ and asymptotic spectra are very similar. The OLES $\tilde{\mathcal{Q}}_{tnt}$ operators are also quite similar to the fourth-order operator, while the $\tilde{\mathcal{Q}}_{nnn}$ operators are significantly different. The reason for this qualitative discrepancy between the operators is that the $\tilde{\mathcal{Q}}_{nnn}$ operator has many more parameters defining it (six) than does $\tilde{\mathcal{Q}}_{tnt}$ (two) because the $\tilde{\mathcal{Q}}_{tnt}$ defined here involve only the two $\tilde{w}_n$ volumes that intersect the volume face through which the flux is estimated. Since the $\tilde{\mathcal{Q}}$ operators are constrained to be second-order approximations, there is only one degree of freedom left to optimize in $\tilde{\mathcal{Q}}_{tnt}$, while there are five in $\tilde{\mathcal{Q}}_{nnn}$.

There are two obvious differences between the spectra of OLES operator $\tilde{\mathcal{Q}}_{nnn}$ and the standard finite-volume scheme shown in Fig. 10. First, the standard fourth-order approximation is identically zero when either of the wavenumbers is $\pm\pi$, which is a consequence of the way the operator is constructed as the product of fourth-order interpolants. This is clearly not true of the OLES operator. Second, the magnitude of the spectral values $\lambda^{\mathcal{Q}}$ is significantly larger in the OLES operator. This is apparent in Fig. 11 where the spectrum along the diagonal from (0,0) to $(\pi,\pi)$ is plotted for the different operators. The optimal operators have a peak that is about 70% larger than the fourth-order operator, and occur at larger wavenumber, right at the boundary between unaliased and aliased wavenumbers. For very small wavenumbers, the slope of the OLES spectral plots is one as is required by the fact that it is a second-order approximation to the Navier–Stokes convective term, but unlike the fourth-order approximation and the exact Navier–Stokes operator, the slope of the spectrum increases to approximately 1.2 for intermediate wavenumbers. It is not yet clear why an operator with these properties is appropriate for a LES, although it is interesting that OLES spectra along the diagonal are closer than the fourth-order operator to the exact Navier–Stokes spectrum in the unaliased range. Regardless, the differences between the OLES operator and the fourth-order or exact Navier–Stokes operators should be understood as part of the model for subgrid effects. Further analysis of the OLES operators and their properties will be valuable for formulating generalizations.

### C. Role of the three-point third-order correlation

As is clear from Sec. III A, the most difficult modeling task involved in formulating the models presented here is the representation of the three-point third-order correlation, which is used to determine $I^3$. The representation for this quantity was feasible[15] only because of the assumption of small-scale isotropy. In more complex situations in which the

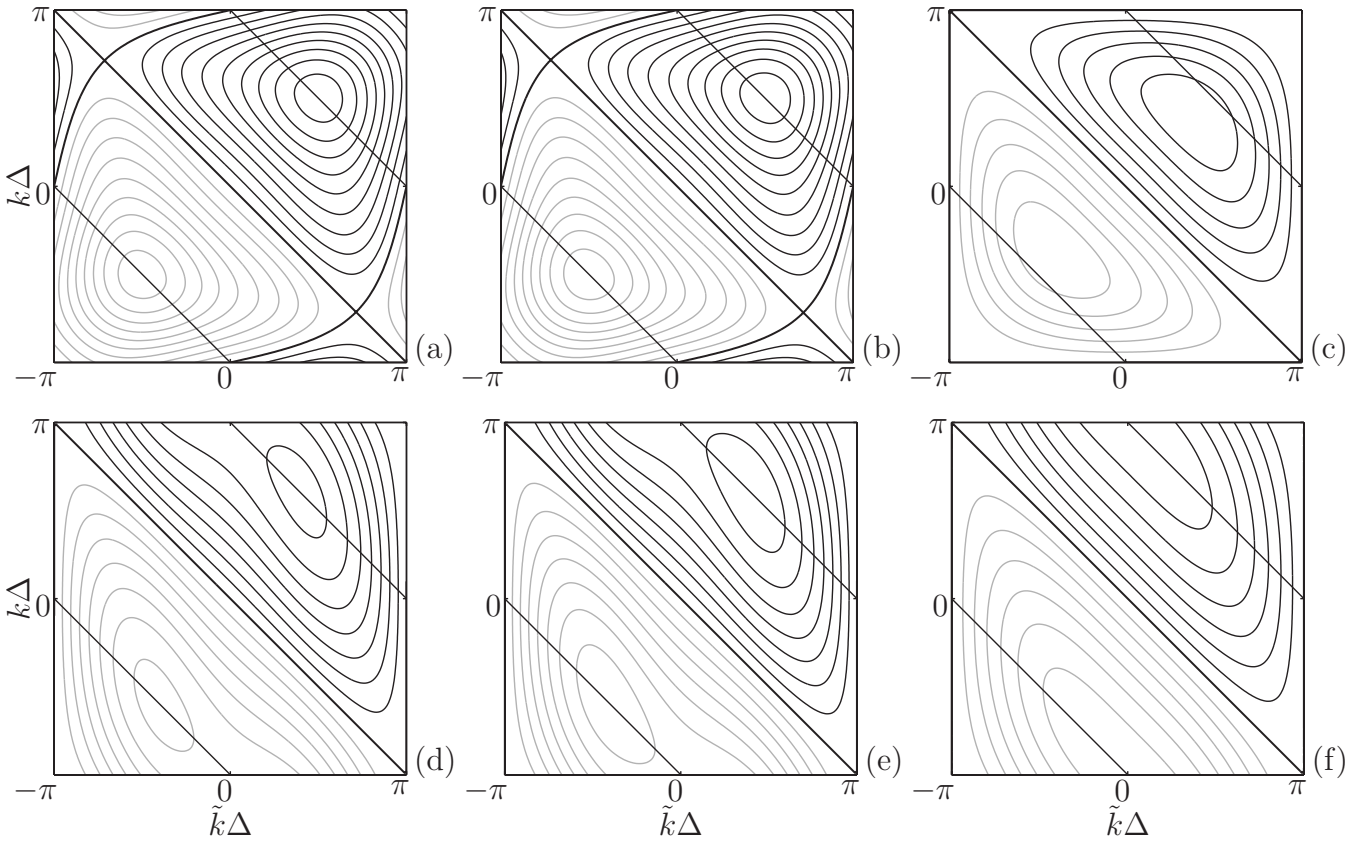


FIG. 10. Bilinear spectra [(a)–(c)] $-i\lambda_n^Q(k,\tilde{k})$ and [(d)–(f)] $-i\lambda_l^Q(k,\tilde{k})$. The spectra are for asymptotic optimal [(a) and (d)], $32^3$ optimal [(b) and (e)], and fourth-order operators [(c) and (f)]. Black contours are positive and gray are negative. The heavy contours indicate the zero level. Contour values are incremented by 0.3.

small-scale isotropy assumption would not be valid, detailed modeling of the three-point third-order correlation will be much more difficult, if not infeasible. It is interesting, then, to consider how important this quantity is to the modeling and thus how well it needs to be known.

The primary use for $I^3$ is in determining the modeling kernels. In particular, it appears in the terms that couple the equations for the quadratic and linear kernels [Eqs. (46) and (47)]. The coupling is most important in the equation for the linear kernels [Eq. (46)], as the coupling term in the quadratic equation (47) is second order in $\gamma^{2/3}$. To understand the role of this term, consider the evolution equation derived from Eq. (2) for $\langle \bar{u}_l^{v_3'} \bar{u}_i^{v'} \rangle$, which is the two-point correlation of the filtered (i.e., volume-averaged) velocity. The contribution from the nonlinear terms $\mathcal{F}_i^s$ in this equation is given by

$$-\sum_s \langle \bar{u}_l^{v_3'} \mathcal{F}_i^{4s} \rangle = -\sum_s I_{li}^1(v_3,s), \tag{78}$$

which, when normalized as in Sec. III B, is the sum (over $s$) of the left hand side of Eq. (46). The terms on the right hand side of Eq. (46) can thus be interpreted as the expected contributions of the linear and quadratic part of the model flux to the evolution of the two-point correlations, with the quadratic contribution being the term of interest here, by involving $I^3$. Indeed, Eq. (46) can be interpreted as a condition requiring that the contributions of the model to the filtered two-point correlation be the same as that for true turbulence, at least for separations included in the kernel stencil (see Ref. 8). The critical role of $I^3$, then, is to measure this contribution of the quadratic part of the model. In particular, when $v_3 = v$ (the single point correlation), $I^3$ is measuring the contribution of the quadratic model term to the transfer of energy to the small scales, which is the basis of the dissipation analysis in Sec. V A.

The analysis of Sec. V A, however, showed that the contribution to the dissipation (transfer to small scales) of the

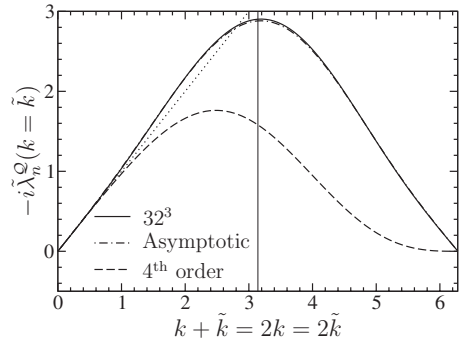


FIG. 11. The bilinear spectra $\lambda_n^Q(k,\tilde{k})$ for the normal quadratic operator along the diagonal $k=\tilde{k}$. Shown are the spectra for the asymptotic operators ($\gamma=0$), those determined for a $32^3$ grid ($\gamma=0.08$), and those for a standard fourth-order operator. The vertical line at $k+\tilde{k}=\pi$ indicates the boundary between aliased (right) and unaliased (left) portions of the spectrum, and the dotted line is the spectrum of the exact Navier–Stokes operator.

TABLE IV. Contributions to dissipation of the quadratic ($\epsilon^{\mathcal{Q}}$) and linear ($\epsilon^{\mathcal{L}}$) portions of the asymptotic LES operators determined by neglecting the $I^3$ terms in Eqs. (63) and (67) for flux of the normal momentum (normal) and tangential momentum (tangential). The sum $3N+6T$ signifies three times the normal contribution plus six times the tangential, which represents the contributions to the total dissipation of kinetic energy ($\epsilon$).

| Operator | $\epsilon^{\mathcal{Q}}/\epsilon$ | $\epsilon^{\mathcal{L}}/\epsilon$ | $(\epsilon^{\mathcal{Q}}+\epsilon^{\mathcal{L}})/\epsilon$ |
|---|---|---|---|
| Normal | −0.003 251 | −0.133 333 | −0.136 584 |
| Tangential | −0.010 070 | −0.100 000 | −0.110 070 |
| $3N+6T$ | −0.070 174 | −1.000 000 | −1.070 174 |

asymptotic quadratic model term is actually quite small (about 2%, see Table III). If this were generally indicative of the contribution of the $I^3$ terms to the estimation equations, then it would be reasonable to neglect them, greatly simplifying the modeling problem by making it largely unnecessary to develop a model for the three-point third-order correlation.

To explore this possibility, a set of asymptotic kernels was determined by neglecting the $I^3$ terms in the asymptotic equations (63) and (67). As indicated in Table IV, the normal and tangential linear operators become somewhat less and more dissipative, respectively. The net result is that the overall model is 7% overdissipative, with the balance between contributions from normal and tangential components tilted toward the tangential components, relative to the exact distribution. Neglect of the $I^3$ term may also affect the scale distribution of the dissipation. LESs with these modified kernels were performed, and the results for the three dimensional spectrum and third-order structure function are shown in Fig. 12. The spectrum in the simulation that neglected the $I^3$ terms differs from that obtained with the usual asymptotic kernels in the highest octave of wavenumbers, with an upturn followed by a sharper roll-off. This demonstrates the role of the $I^3$ terms in shaping the scale distribution of the dissipation provided by the linear part of the model, in addition to the overall dissipation rate described above. The effect of neglecting the $I^3$ terms on the simulated third-order structure function is pronounced only at separations greater than $4\Delta$, for reasons that are not clear.

The importance of these differences to a practical LES can be debated. In general, whether or not the additional modeling error introduced by neglecting the $I^3$ terms is acceptable will depend on the goals of a particular simulation. The modest impact on the LES results in this case suggests that neglecting the $I^3$ terms or crudely modeling the underlying three-point third-order correlation (e.g., to account for anisotropy) may be a viable strategy in more complex flow situations. However, one must be cautious in this conclusion since in more complex situations, the quadratic operator may not behave as well, requiring a more tailored correction with the linear term, which would be determined through the $I^3$ terms.

Finally, in the LES performed here, there is one further role that the three-point third-order correlation plays through $I^3$, that is, dynamically determining the dissipation rate $\epsilon$ as described in Sec. IV A. While this approach is very effective, if one is seeking to reduce the need to model the three-point third-order correlation, dissipation could also be estimated from the two-point second-order correlation and $I^2$, although this has not been explored here.

## VI. CONCLUSIONS

It was shown in Ref. 11 that finite-volume OLES models, which account for the effects of the Navier–Stokes dynamics, subgrid modeling, and numerical discretization, give good *a posteriori* results and perform better than the dynamic Smagorinsky models. The inputs required by the finite-volume OLES models may be expressed as volume and surface integrals of multipoint velocity correlations of second, third, and fourth orders. In previous work,[11] these correlations were obtained from DNS, which restricts the usefulness of the technique.

In this paper, it is shown that the correlations required for the finite-volume OLES formulation can be obtained from the Kolmogorov inertial range theory, small-scale isot-

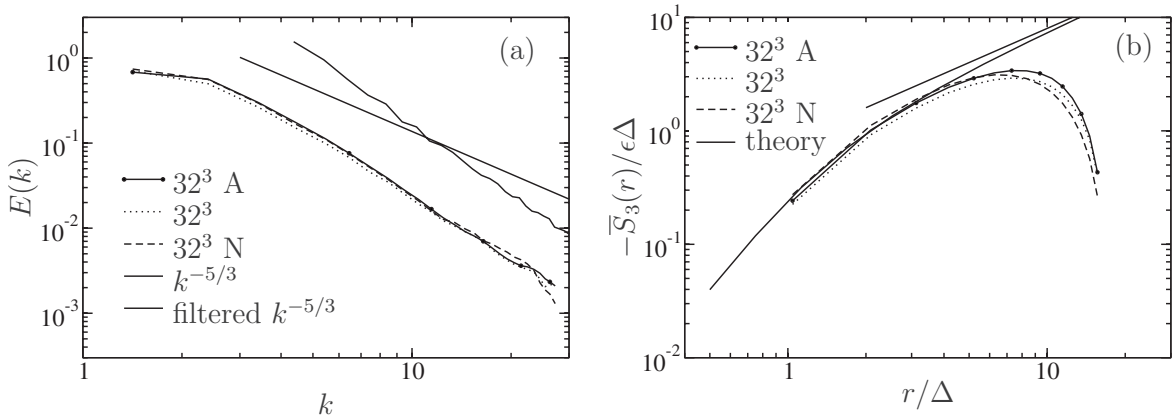


FIG. 12. Three-dimensional energy spectra (a) and third-order structure functions (b) from OLES of isotropic turbulence at infinite Reynolds with resolution of $32^3$ ($\gamma$=0.08). Compared are results using the finite $\gamma$ kernels, asymptotic kernels (signified with A), and asymptotic kernels generated by neglecting the $I^3$ terms in Eqs. (63) and (67) (signified with "N"). Solid lines in (a) and (b) are as in Fig. 6.

ropy, and the quasinormal approximation. Further, it is shown that LES models resulting from these correlations perform well. These approximations will be valid provided the turbulence at the filter scale and smaller is locally homogeneous and isotropic. Except for very near walls and other strong inhomogeneities, this is expected to be a good approximation provided the Reynolds number is sufficiently high and the filter width is sufficiently small.

The finite-volume OLES models developed here are expressed as discrete quadratic and linear operators that represent the convective momentum flux. These operators depend explicitly on two flow dependent parameters: the dissipation rate $\epsilon$ and the nondimensional parameter $\gamma=\Delta\epsilon/u^3$ (the ratio of the grid size $\Delta$ to the large turbulence scale). The modeling approach allows the parameters $\epsilon$ and $u^2$ to be determined dynamically and accurately in a running LES. However it was also found that asymptotic operators for $\gamma\to 0$ yield results consistent with the finite $\gamma$ operators with $\gamma$ as large as 0.08. In most cases, therefore, the asymptotic operators are sufficiently accurate, meaning that only $\epsilon$ needs be determined dynamically. The process for determining $\epsilon$ [Eq. (57)] is considerably simpler than the usual dynamic procedure,[35] as no test filter is required.

The quadratic and linear operators arising from the LES optimization are broadly similar to common finite-volume operators. However, there are significant quantitative differences between the OLES operators and standard finite-volume operators, which should be interpreted as part of the model for the effects of subgrid scales. The linear part of the operators, which plays the role of the subgrid stress model by dissipating resolved energy, are different for the normal and tangential velocity components in any grid direction, with the tangential-component dissipation significantly higher at high wavenumbers than a standard fourth-order approximation to the second derivative. This is one of the features of the OLES approach; the spectral distribution of subgrid dissipation is tailored to be consistent with the statistics of turbulence. Finally, note that the quadratic OLES operators on average produce resolved-scale energy and the linear operators dissipate energy. The dissipation of the linear term is determined to ensure that the combined contributions of quadratic and linear terms to the resolved energy evolution match the required total dissipation.

These results indicate that practical finite-volume OLES models can be formulated without DNS correlation inputs, at least for the circumstances for which most LES models are designed (small-scale isotropy). The advantage of the current formulation is that it allows the effects of subgrid turbulence and numerical discretization to be treated in a unified way and consistent with the statistical properties of turbulence. It is both remarkable and encouraging that the simple considerations employed here are sufficient for this modeling. All of these provide motivation for further development, implementation, and testing of OLES models in a broad class of turbulent flows.

Several immediate generalizations are possible using the isotropic statistical models introduced here. These include LES of scalar transport and modeling on anisotropic and inhomogeneous grids, as one would encounter in most applications. Also important is the generalization to anisotropic correlations for LES models applicable when isotropy at the grid scale is not a valid assumption. This occurs, for example, in near-wall turbulence. Isotropy places a strong constraint on the form of the multipoint correlations. Without isotropy, even the two-point second-order correlation is difficult to represent (see Ref. 37 and the references therein). The possibility raised in Sec. V C that the $I^3$ contribution to the OLES estimation equations might be neglected or crudely modeled is thus particularly important since the underlying three-point third-order correlation is the most difficult to model. However, the robustness of this result to anisotropy and inhomogeneity of the turbulence and the LES grid is far from clear and will need to be evaluated.

## ACKNOWLEDGMENTS

The research reported here was supported under NSF Grant Nos. CTS-001435, CTS-03-52552, and OCI-07-49286 and AFOSR Grant Nos. F49620-01-1-0181, FA9550-04-1-0032, and FA9550-07-1-0197, and by the Center for Simulation of Advanced Rockets, which is funded by the Department of Energy through University of California Grant No. B341494. Partial support for R.D.M. was provided by the MEC in Spain through their Sabbatical Program. This support is gratefully acknowledged. We also benefited from many discussions with Professor Javier Jiménez and Professor Ron Adrian.

## APPENDIX A: FORMULATION OF MEAN AND CROSS TERMS

In this appendix, we examine the treatment of the flux terms involving the mean velocity [$\mathcal{F}_i^{1s}$, $\mathcal{F}_i^{2s}$, and $\mathcal{F}_i^{3s}$, see Eqs. (12)–(14)]. Since $\mathcal{F}_i^{1s}$ is deterministic, it must be determined by means other than stochastic estimation. In a LES, it is reasonable to expect that the mean velocity will be well resolved in the LES representation (although possibly not near walls). Under these assumptions, $\mathcal{F}_i^{1s}$ can be approximated using standard finite-volume schemes operating on the mean LES velocities $W_i^v$. In particular, finite-volume schemes are commonly written in terms of reconstructed surface velocities,

$$\mathcal{F}_i^{1s} \approx A_s \tilde{U}_i \tilde{U}_s, \tag{A1}$$

where $\tilde{U}_s$ is the reconstructed velocity component normal to the surface $s$ and $A_s$ is the area of surface $s$. The reconstructed surface velocities are approximated as

$$\tilde{U}_i \approx \sum_{v_1} \tilde{\mathcal{P}}(s,v_1) W_i^{v_1}, \quad \tilde{U}_s \approx \sum_{v_1} \tilde{\mathcal{R}}(s,v_1) W_s^{v_1}, \tag{A2}$$

where $\tilde{\mathcal{P}}$ and $\tilde{\mathcal{R}}$ are sets of coefficients chosen to yield reconstructions accurate to some given order of accuracy (say second order). In general, the reconstruction for $\tilde{U}_i$ and $\tilde{U}_s$ may be different, for example, to accommodate a staggered grid. As long as approximation (A2) is at least second order, then Eq. (A1) will also be second order (see below). This error is due solely to numerical discretization and can be analyzed as such.

To model the cross-term fluxes $\mathcal{F}_i^{2s}$ and $\mathcal{F}_i^{3s}$, the reconstructed mean velocity can again be used, under the assumption that the mean velocity is well resolved,

$$\mathcal{F}_i^{2s} \approx A_s \widetilde{U}_i \widetilde{u}_s', \quad \mathcal{F}_i^{3s} \approx A_s \widetilde{u}_i' \widetilde{U}_s, \tag{A3}$$

where the surface averaged velocity fluctuations given by

$$\widetilde{u}_i' = \frac{1}{A_s}\int_s u_i' d\mathbf{x}, \quad \widetilde{u}_s' = \frac{1}{A_s}\int_s u_j' n_j^s d\mathbf{x} \tag{A4}$$

are to be modeled using OLES techniques. To this end, the following estimation equations can be used:

$$\widetilde{u}_i' \approx \sum_{v_1} \mathcal{P}_{ij}(s,v_1) w_j^{v_1}, \tag{A5}$$

$$\widetilde{u}_s' \approx \sum_{v_1} \mathcal{R}_j(s,v_1) w_j^{v_1}, \tag{A6}$$

$$\langle \widetilde{u}_i' \vec{u}_k^{v_2\prime} \rangle = \sum_{v_1} \mathcal{P}_{ij}(s,v_1) \langle \vec{u}_j^{v_1\prime} \vec{u}_k^{v_2\prime} \rangle, \tag{A7}$$

$$\langle \widetilde{u}_s' \vec{u}_k^{v_2\prime} \rangle = \sum_{v_1} \mathcal{R}_j(s,v_1) \langle \vec{u}_j^{v_1\prime} \vec{u}_k^{v_2\prime} \rangle. \tag{A8}$$

The estimates need only to be linear with no mean term because $\widetilde{u}_i'$ and $\widetilde{u}_s'$ are linear in the velocity with zero mean.

In developing the approximations/models [Eqs. (A1), (A3), and (A4)], three distinct errors are committed: the numerical reconstruction error incurred in Eq. (A2), the error in approximating $\mathcal{F}_i^{2s}$ and $\mathcal{F}_i^{3s}$ in the split form [Eq. (A3)], and the modeling error in the stochastic models (A5) and (A6).

To analyze these errors, we introduce a decomposition (in addition to the Reynolds decomposition) into the surface average $\widetilde{(\cdot)}$ and surface variation $\hat{(\cdot)}$ for the surface over which the flux is to be determined. Thus, a function $f$ is decomposed as $f=\widetilde{f}+\hat{f}$. The surface average mean velocity $\widetilde{U}_i$ is precisely the reconstructed quantity needed in Eqs. (A1) and (A3).

The error $E_1$ in approximating $\mathcal{F}_i^{1s}$ with Eq. (A1) is given by

$$E_1 = \frac{1}{A_s}\int_s U_i U_s d\mathbf{x} - \widetilde{U}_i \widetilde{U}_s = \frac{1}{A_s}\int_s \hat{U}_i \hat{U}_s d\mathbf{x}. \tag{A9}$$

Since the flux surface has linear dimensions of the order of the filter width, $\Delta$, $|\hat{U}_i| < \widetilde{C}\Delta$, for some constant $\widetilde{C}$ independent of $\Delta$ (but depending on $U_i$). This arises because if $\hat{U}_i$ is sufficiently smooth on the surface (as expected for the mean velocity), the mean value theorem guarantees that any point on the surface can only be of order $\Delta$ away from the point where $\hat{U}_i$ is zero, ensuring that $\hat{U}_i$ is no more than order $\Delta$ on the surface. The error $E_1$ then scales as $\Delta^2$, which is therefore second order. If the finite-volume approximation to $\widetilde{U}_i$ is also second order, the overall approximation to $\mathcal{F}_i^{1s}$ will be second order (this is the usual analysis for finite-volume methods).

The errors $E_2$ and $E_3$ in approximating $\mathcal{F}_i^{2s}$ and $\mathcal{F}_i^{3s}$ using Eq. (A3) can be analyzed similarly. Here, consider $E_2$ ($E_3$ is analogous), which is written as

$$E_2 = \frac{1}{A_s}\int_s U_i u_s' d\mathbf{x} - \widetilde{U}_i \widetilde{u}_s' d\mathbf{x} = \frac{1}{A_s}\int_s \hat{U}_i \hat{u}_s' d\mathbf{x}. \tag{A10}$$

Because $u'$ is stochastic, $E_2$ is as well, and we consider its statistics,

$$\langle E_2 \rangle = \frac{1}{A_s}\int_s \hat{U}_i \langle \hat{u}_s' \rangle d\mathbf{x} = 0, \tag{A11}$$

$$\langle E_2^2 \rangle = \frac{1}{A_s^2}\int_s \int_s \hat{U}_\alpha(\mathbf{x}) \hat{U}_\alpha(\mathbf{x}') \langle \hat{u}_s'(\mathbf{x}) \hat{u}_s'(\mathbf{x}') \rangle d\mathbf{x} d\mathbf{x}'. \tag{A12}$$

A bound is already available for $\hat{U}_\alpha$ on the surface $s$ so all that is needed is to bound $\langle \hat{u}_s'(\mathbf{x}) \hat{u}_s'(\mathbf{x}') \rangle$. To this end we write

$$\begin{aligned}\langle \hat{u}_s'(\mathbf{x}) \hat{u}_s'(\mathbf{x}') \rangle = {} & \langle u_s'(\mathbf{x}) u_s'(\mathbf{x}') \rangle - \langle u'(\mathbf{x}) \widetilde{u}_s'(\mathbf{x}') \rangle \\ & - \langle u'(\mathbf{x}') \widetilde{u}_s'(\mathbf{x}) \rangle + \langle \widetilde{u}_s'(\mathbf{x}) \widetilde{u}_s'(\mathbf{x}) \rangle,\end{aligned} \tag{A13}$$

which can be written in terms of the two-point correlation $R_{ss}(\mathbf{r})$,

$$\begin{aligned}\langle \hat{u}_s'(\mathbf{x}) \hat{u}_s'(\mathbf{x}') \rangle = {} & R_{ss}(\mathbf{r}) - \frac{1}{A_s}\int_s R_{ss}(\mathbf{r}) d\mathbf{x} - \frac{1}{A_s}\int_s R_{ss}(\mathbf{r}) d\mathbf{x}' \\ & + \frac{1}{A_s^2}\int_s \int_s R_{ss}(\mathbf{r}) d\mathbf{x} d\mathbf{x}',\end{aligned} \tag{A14}$$

where $\mathbf{r}=\mathbf{x}-\mathbf{x}'$. Now assuming that for separations of order $\Delta$, the two-point correlation is isotropic and that $\Delta$ is in the inertial range, the Kolmogorov expression (32) can be used for $R_{ss}$. The constant term $(u^2)$ then drops out, and the remaining term scales like $R_{ss}-u^2 \sim |\mathbf{r}|^{2/3}$. Because the integrals are over surfaces of size $\Delta$, the required bound is

$$\langle \hat{u}_s'(\mathbf{x}) \hat{u}_s'(\mathbf{x}') \rangle < \widetilde{C}\Delta^{2/3}. \tag{A15}$$

Combining this with the previous bound on $\hat{U}_i < \widetilde{C}\Delta$, a bound on $\langle E_2^2 \rangle < \hat{C}\Delta^{8/3}$ is obtained. The rms $E_2$ thus scales no worse than $\Delta^{4/3}$. Identical arguments lead to identical results for $E_3$.

The modeling error for $\mathcal{F}_i^{2s}$ and $\mathcal{F}_i^{3s}$ is more difficult to determine. The deviation of $\widetilde{u}'$ about its estimate is bounded by $\Delta^{1/3}$ [Eq. (A15)], but this is not the error of interest. The relevant error is the difference between the OLES estimate and the ideal estimate given by the conditional average $\langle \widetilde{u}_i' \,|\, \bar{u}=w \rangle$. The dependence of this error on $\Delta$ is not known but it is certainly bounded by the deviation of $\widetilde{u}'$ and $\Delta^{1/3}$. While there is no proof, it is reasonable to expect that for sufficiently small $\Delta$, the error in the mixed term will be dominated by modeling errors, justifying the use of the split form [Eq. (A3)].

TABLE V. Values of the elements of $\tilde{I}^1$ for a $1\times1\times4$ stencil, with volume labels as defined in Fig. 4. The values of $\tilde{I}^1$ for volumes not listed are determined from the symmetry $\tilde{I}^1_{\alpha\alpha}(-v_1,s)=-\tilde{I}^1_{\alpha\alpha}(v_1,s)$.

| $v_1$ | $\tilde{I}^1_{nn}(v_1,s)$ | $\tilde{I}^1_{tt}(v_1,s)$ |
|---|---|---|
| 2 | $-\frac{1}{5}$ | $-\frac{3}{20}$ |
| 1 | $-\frac{1}{15}$ | $-\frac{1}{20}$ |

## APPENDIX B: SCALED CORRELATIONS AND FLUXES

Presented in this appendix are the scaled correlations $\tilde{I}^1-\tilde{I}^5$ for the $1\times1\times4$ OLES stencils used in the LES presented in Sec. IV C. Since these correlations depend on $\gamma$ as well as the geometry of the stencils, the correlations are reported in terms of their expansion with respect to $\gamma$, as defined in Eqs. (48)–(52).

The correlations are defined in terms of the volumes in the stencil shown in Fig. 4 to estimate the flux through the face between volume 1 and $-1$. The grid is staggered, and so depending on the flux being determined, different volumes are involved. When estimating the flux of normal momentum, the volumes $\pm1$ and $\pm2$ are used, and they are volumes in the grid for the velocity component in the normal direction. When estimating flux of the tangential momentum, volumes $\pm1$ and $\pm2$, which are, in that case, on the tangential velocity grid, are used, as is volume 0, which is on the normal velocity grid. The normal velocity cell immediately below 0 is also used (not shown), but its correlations with the other volumes are the same as for volume 0.

Isotropy and homogeneity introduce symmetries into the correlations, which have been used to reduce the amount of data that must be reported. For example, isotropy implies that correlations in the stencil defined above are the same, regardless of the orientation of the face being considered. Furthermore, isotropy and homogeneity imply symmetries in the correlation values within a single stencil. Through consideration of these symmetries, the correlation values reported here are sufficient to determine all the correlations and estimation kernels used in this paper. However, values for $\tilde{I}^5$ are not reported because through the use of the quasi-normal approximation, $\tilde{I}^5$ can be written in terms of $\tilde{I}^2$, as follows:

$$I^5_{ijkl}(v_1,v_2,v_3,v_4)\approx I^2_{ij}(v_1,v_2)I^2_{kl}(v_3,v_4)+I^2_{ik}(v_1,v_3)I^2_{jl}(v_2,v_4)+I^2_{il}(v_3,v_4)I^2_{jk}(v_2,v_3). \tag{B1}$$

TABLE VI. Values of the elements of $\tilde{I}^{20}$ and $\tilde{I}^{21}$ for a $1\times1\times4$ stencil. For $\tilde{I}_{nn}$ and $\tilde{I}_{tt}$, volume label $v_1\pm m\Delta$ indicates a volume separated by $m$ volumes in the normal direction, with, for example, $v_1+0\Delta$ signifying $v_1$ and $v_1\pm\Delta$ signifying the neighboring volume (in either direction). For $\tilde{I}_{nt}$, the volume labels are as defined in Fig. 4.

| $m$ | $\tilde{I}^{20}_{nn}(v_1,v_1\pm m\Delta)$ | $\tilde{I}^{20}_{tt}(v_1,v_1\pm m\Delta)$ | $\tilde{I}^{20}_{nt}(0,\pm m)$ |
|---|---|---|---|
| * | 1 | 1 | 0 |
| | $\tilde{I}^{21}_{nn}(v_1,v_1\pm m\Delta)$ | $\tilde{I}^{21}_{tt}(v_1,v_1\pm m\Delta)$ | $\tilde{I}^{21}_{nt}(0,\pm m)$ |
| 0 | −0.911 84 | −0.911 84 | ⋯ |
| 1 | −1.187 93 | −1.414 11 | −0.068 01 |
| 2 | −1.667 19 | −2.144 92 | −0.155 31 |
| 3 | −2.126 94 | −2.789 51 | ⋯ |

TABLE VII. Values of the elements of $\tilde{I}^3$ for a $1\times1\times4$ stencil, with volume labels as defined in Fig. 4. The value of $\tilde{I}^3$ for volumes not listed here are determined from the symmetry $\tilde{I}^3_{\alpha n\alpha}(s,-v_1,-v_2,-v_3)=\tilde{I}^3_{\alpha n\alpha}(s,v_1,v_2,v_3)$, the fact that $\tilde{I}^3_{nnn}$ is invariant with respect to permutation of the volume order, and that $\tilde{I}^3_{tnt}$ is invariant to a swap of $v_1$ and $v_3$.

| $v_1$ | $v_2$ | $v_3$ | $\tilde{I}^3_{nnn}(v_1,v_2,v_3)$ |
|---|---|---|---|
| 2 | 2 | 1 | 0.040 242 |
| 2 | 2 | −1 | 0.157 165 |
| 2 | 2 | −2 | 0.287 861 |
| 2 | 1 | 1 | −0.040 242 |
| 2 | 1 | −1 | 0.0 |
| 2 | 1 | −2 | 0.122 190 |
| 2 | −1 | −1 | −0.157 165 |
| 1 | 1 | −1 | 0.040 242 |
| $v_1$ | $v_2$ | $v_3$ | $\tilde{I}^3_{tnt}(v_1,v_2,v_3)$ |
| 2 | 0 | 2 | −0.053 828 |
| 2 | 0 | 1 | −0.096 262 |
| 2 | 0 | −1 | −0.082 526 |
| 2 | 0 | −2 | 0.0 |
| 1 | 0 | 1 | −0.010 838 |
| 1 | 0 | −1 | 0.0 |

TABLE VIII. Values of the elements of $\tilde{I}^{40}$, $\tilde{I}^{41}$, and $\tilde{I}^{42}$ for a $1\times1\times4$ stencil, with volume labels as defined in Fig. 4. The value of $\tilde{I}^{4\beta}$ for volumes not listed here is determined from the symmetry $\tilde{I}^4_{n\alpha\alpha}(-v_1,-v_2,s)=\tilde{I}^4_{n\alpha\alpha}(v_1,v_2,s)$.

| $v_1$ | $v_2$ | $\tilde{I}^{40}_{nnn}(v_1,v_2,s)$ | $\tilde{I}^{40}_{ntt}(v_1,v_2,s)$ |
|---|---|---|---|
| * | * | 3 | 1 |
| $v_1$ | $v_2$ | $\tilde{I}^{41}_{nnn}(v_1,v_2,s)$ | $\tilde{I}^{42}_{nnn}(v_1,v_2,s)$ |
| 2 | 2 | −6.615 37 | 4.068 73 |
| 2 | 1 | −5.983 47 | 2.776 56 |
| 2 | −1 | −6.462 74 | 2.776 56 |
| 2 | −2 | −7.830 50 | 4.068 73 |
| 1 | 1 | −4.799 30 | 1.899 29 |
| 1 | −1 | −5.075 44 | 1.899 29 |
| $v_1$ | $v_2$ | $\tilde{I}^{41}_{ntt}(v_1,v_2,s)$ | $\tilde{I}^{42}_{ntt}(v_1,v_2,s)$ |
| 0 | 2 | −2.836 97 | 1.871 62 |
| 0 | 1 | −2.076 08 | 1.080 48 |

The values of the correlation integrals are given in Tables V–VIII. These correlations were computed as integrals of the multipoint correlations. These are high-dimensional integrals (for example, $I^3$ is an integral in nine dimensions) and adaptive quadrature[34] implemented in the routine DCUHRE (available at http://portal.acm.org) was used to perform the quadrature with an error tolerance of $10^{-7}$.


[1] R. Rogallo and P. Moin, "Numerical simulation of turbulent flows," Annu. Rev. Fluid Mech. **16**, 99 (1984).
[2] M. Lesieur and O. Métais, "New trends in large-eddy simulations of turbulence," Annu. Rev. Fluid Mech. **28**, 45 (1996).
[3] C. Meneveau and J. Katz, "Scale-invariance and turbulence models for large-eddy simulation," Annu. Rev. Fluid Mech. **32**, 1 (2000).
[4] K. R. Sreenivasan and R. A. Antonia, "The phenomenology of small-scale turbulence," Annu. Rev. Fluid Mech. **29**, 435 (1997).
[5] S. Ghosal, "An analysis of numerical errors in large-eddy simulations of turbulence," J. Comput. Phys. **125**, 187 (1996).
[6] A. G. Kravchenko and P. Moin, "On the effect of numerical errors in large eddy simulations of turbulent flows," J. Comput. Phys. **131**, 310 (1997).
[7] U. Piomelli and E. Balaras, "Wall-layer models for large-eddy simulations," Annu. Rev. Fluid Mech. **34**, 349 (2002).
[8] J. A. Langford and R. D. Moser, "Optimal LES formulations for isotropic turbulence," J. Fluid Mech. **398**, 321 (1999).
[9] J. A. Langford and R. D. Moser, "Optimal large-eddy simulation results for isotropic turbulence," J. Fluid Mech. **521**, 273 (2004).
[10] S. Volker, P. Venugopal, and R. D. Moser, "Optimal large eddy simulation of turbulent channel flow based on direct numerical simulation statistical data," Phys. Fluids **14**, 3675 (2002).
[11] P. S. Zandonade, J. A. Langford, and R. D. Moser, "Finite-volume optimal large-eddy simulation of isotropic turbulence," Phys. Fluids **16**, 2255 (2004).
[12] D. Carati, G. S. Winckelmans, and H. Jeanmart, "On the modelling of the subgrid-scale and filtered-scale stress tensors in large-eddy simulation," J. Fluid Mech. **441**, 119 (2001).
[13] T. J. R. Hughes, L. Mazzei, A. A. Oberai, and A. A. Wray, "The multiscale formulation of large eddy simulation: Decay of homogeneous isotropic turbulence," Phys. Fluids **13**, 505 (2001).
[14] T. J. R. Hughes, A. A. Oberai, and L. Mazzei, "Large eddy simulation of turbulent channel flows by the variational multiscale method," Phys. Fluids **13**, 1784 (2001).
[15] H. Chang and R. D. Moser, "An inertial range model for the three-point third-order velocity correlation," Phys. Fluids **19**, 105111 (2007).
[16] S. B. Pope, *Turbulent Flows* (Cambridge University Press, Cambridge, 2000).
[17] R. Adrian, B. Jones, M. Chung, Y. Hassan, C. Nithianandan, and A. Tung, "Approximation of turbulent conditional averages by stochastic estimation," Phys. Fluids A **1**, 992 (1989).
[18] R. Adrian, "On the role of conditional averages in turbulence theory," in *Turbulence in Liquids*, edited by J. Zakin and G. Patterson (Science, Princeton, NJ, 1977), pp. 323–332.
[19] R. Adrian, "Stochastic estimation of sub-grid scale motions," Appl. Mech. Rev. **43**, S214 (1990).
[20] A. Das and R. D. Moser, "Optimal large eddy simulation of forced Burgers' equation," Phys. Fluids **14**, 4344 (2002).
[21] J. A. Langford and R. D. Moser, "Breakdown of continuity in large-eddy simulation," Phys. Fluids **13**, 1524 (2001).
[22] As an alternative to the decomposition of the velocity into mean and its fluctuating components, one can also consider a more general partition of the velocity into a resolved-scale quantity and its complement. The tools developed in this section can be easily generalized to this alternative decomposition. For this alternative decomposition, $\langle \mathcal{F}_i^s \rangle$ will also include contributions from $\langle \mathcal{F}_i^{2s} \rangle$ and $\langle \mathcal{F}_i^{3s} \rangle$.
[23] A. N. Kolmogorov, "The local structure of turbulence in incompressible viscous fluid for very large Reynolds numbers," C. R. Acad. Sci. URSS **30**, 301 (1941) [reprinted in Proc. R. Soc. London, Ser. A **434**, 9 (1991)].
[24] A. N. Kolmogorov, "Dissipation of energy in locally isotropic turbulence," Dokl. Akad. Nauk SSSR **32**, 16 (1941) [reprinted in Proc. R. Soc. London, Ser. A **434**, 15 (1991)].
[25] T. von Kármán and L. Howarth, "On the statistical theory of isotropic turbulence," Proc. R. Soc. London, Ser. A **164**, 192 (1938).
[26] G. K. Batchelor, *The Theory of Homogeneous Turbulence* (Cambridge University Press, Cambridge, 1953), p. 53.
[27] A. S. Monin and A. M. Yaglom, *Statistical Fluid Mechanics: Mechanics of Turbulence* (Dover, New York, 1975), Vol. II, p. 70.
[28] R. H. Kraichnan, "Relation of fourth-order to second-order moments in stationary isotropic turbulence," Phys. Rev. **107**, 1485 (1957).
[29] Y. Ogura, "A consequence of the zero-fourth-cumulant approximation in the decay of isotropic turbulence," J. Fluid Mech. **16**, 33 (1963).
[30] S. Orszag, "Analytical theories of turbulence," J. Fluid Mech. **41**, 363 (1970).
[31] M. Lesieur, *Turbulence in Fluids*, 3rd ed. (Kluwer Academic, Dordrecht, 1997).
[32] P. Vedula, R. D. Moser, and P. S. Zandonade, "On the validity of quasi-normal approximation in turbulent channel flow," Phys. Fluids **17**, 055106 (2005).
[33] I. Proudman and W. H. Reid, "On the decay of a normally distributed and homogeneous turbulent velocity field," Philos. Trans. R. Soc. London, Ser. A **247**, 163 (1954).
[34] J. Berntsen, T. O. Espeld, and A. Genz, "DCUHRE: An adaptive multidimensional integration routine for a vector of integrals," ACM Trans. Math. Softw. **17**, 452 (1991).
[35] M. Germano, U. Piomelli, P. Moin, and W. Cabot, "A dynamic subgrid-scale eddy viscosity model," Phys. Fluids A **3**, 1760 (1991).
[36] F. Harlow and J. Welch, "Numerical calculation of time-dependent viscous incompressible flow of fluid with free surface," Phys. Fluids **8**, 2182 (1965).
[37] A. Bhattacharya, S. Kassinos, and R. D. Moser, "Representing anisotropy of two-point second-order turbulence velocity correlations using structure tensors," Phys. Fluids **20**, 101502 (2008).